Sensitivity of an expanded inclusive search for a MiniBooNE-like excess in MicroBooNE data

by

Jennifer B. Tyler

B.S., Point Loma Nazarene University, 2017

M.S., California State University Fresno, 2020

AN ABSTRACT OF A DISSERTATION

submitted in partial fulfillment of the
requirements for the degree

DOCTOR OF PHILOSOPHY

Department of Physics
College of Arts and Sciences

KANSAS STATE UNIVERSITY
Manhattan, Kansas

2026

Abstract

This dissertation presents the results of a study of how sensitive the MicroBooNE experiment is to an excess of neutrino events with the same topology of the currently-unexplained excess of events observed by the MiniBooNE experiment. This is done by a novel analysis in which events are selected from the MicroBooNE simulation data using only information that was available to MiniBooNE. In order to avoid using information unavailable to MiniBooNE, the neutrino energy was reconstructed assuming all events were quasi-elastic electron neutrino scattering.

This study utilizes the Monte Carlo data sets created by MicroBooNE to simulate a subset of the data collected by MicroBooNE from 2015-2021 from a total exposure of the neutrino target of 1.1×10^{21} protons. Some particles are too low velocity to generate Cherenkov radiation in a MiniBooNE-like detector. Therefore, MiniBooNE-like cuts were used to search for the specific topology of one Cherenkov-visible shower and zero Cherenkov-visible muon tracks to simulate the MicroBooNE Monte Carlo coming out of a MiniBooNE-like detector. This gives a better approximation of the original MiniBooNE analysis that identified the low-energy excess while not being constrained by looking at only single channels. The results of this study can now be compared to an analysis of the full MicroBooNE data.

Sensitivity of an expanded inclusive search for a MiniBooNE-like excess in MicroBooNE data

by

Jennifer B. Tyler

B.S., Point Loma Nazarene University, 2017

M.S., California State University Fresno, 2020

A DISSERTATION

submitted in partial fulfillment of the
requirements for the degree

DOCTOR OF PHILOSOPHY

Department of Physics
College of Arts and Sciences

KANSAS STATE UNIVERSITY
Manhattan, Kansas

2026

Approved by:

Major Professor
Glenn Horton-Smith

Copyright

Abstract

This dissertation presents the results of a study of how sensitive the MicroBooNE experiment is to an excess of neutrino events with the same topology of the currently-unexplained excess of events observed by the MiniBooNE experiment. This is done by a novel analysis in which events are selected from the MicroBooNE simulation data using only information that was available to MiniBooNE. In order to avoid using information unavailable to MiniBooNE, the neutrino energy was reconstructed assuming all events were quasi-elastic electron neutrino scattering.

This study utilizes the Monte Carlo data sets created by MicroBooNE to simulate a subset of the data collected by MicroBooNE from 2015-2021 from a total exposure of the neutrino target of 1.1×10^{21} protons. Some particles are too low velocity to generate Cherenkov radiation in a MiniBooNE-like detector. Therefore, MiniBooNE-like cuts were used to search for the specific topology of one Cherenkov-visible shower and zero Cherenkov-visible muon tracks to simulate the MicroBooNE Monte Carlo coming out of a MiniBooNE-like detector. This gives a better approximation of the original MiniBooNE analysis that identified the low-energy excess while not being constrained by looking at only single channels. The results of this study can now be compared to an analysis of the full MicroBooNE data.

Table of Contents

List of Figures

List of Tables

Acknowledgments

The author thanks the entire MicroBooNE collaboration for their support and countless hours spent helping the author get over the finish line. In particular, the author thanks the PeLEE analysis team for providing the code framework that the author used to conduct this analysis, as well as the Oscillation working group conveners. The author also acknowledges and expresses gratitude to the University Research Association Visiting Scholar Program that allowed the author to spend 10 months at Fermi National Accelerator Laboratory working with members of the MicroBooNE Collaboration.

Finally, the author wishes to acknowledge her family for their consistent love and support during this endeavor. There are not adequate words in any language to express the immense love and gratitude she has for her mother and sisters, so the author simply says from the bottom of her heart, “Thank you.”

Dedication

To my mother.

Through all the laughter and all the tears,

Through all the encouragement and all the despair,

Through all the triumphs and all the disappointments,

Thank you for never giving up on me.

And now look,

Your obstinate, head-strong girl

finally has her wings.

Esther 4:14

Joshua 1:9

John 1:5

Chapter 1

Introduction

This dissertation describes a study done in conjunction with the MicroBooNE collaboration in pursuit of determining the nature of the low-energy excess discovered by MiniBooNE. The purpose of this study is to make a determination of the sensitivity to finding a MiniBooNE-like excess in the MicroBooNE data. A detailed description of this study, as well as descriptions of both the MiniBooNE and MicroBooNE experiments are contained herein.

Chapter 2 provides a short history of and background information on neutrinos. Chapter 3 starts with a description of the MiniBooNE detector, in particular the parts of the detector relevant to this study, and will include a discussion of the Cherenkov light physics vitally important to that detector and this study. Chapter 3 concludes with a discussion of MiniBooNE's low-energy excess result. Chapter 4 continues in the same vein about the MicroBooNE detector, and highlights some of the key differences between the two detectors. Chapter 4 also concludes with a discussion of MicroBooNE's results thus far in pursuit of determining the nature of MiniBooNE's low-energy excess.

Next, Chapter 5 describes this study in detail, including the programs used, selections made, and sideband studies. The results of this study are discussed and analyzed in Chapter 6. A discussion of the uncertainties are also included here. Chapter 7 finishes this dissertation with a sensitivity discussion, final conclusions, and next steps for this study.

In Appendix A, the reader can find the plots for different variables studied during the various stages of selection determination, and the effects of each selection on the different variables. More detailed sideband study plots can be found in Appendix B, including the neutral pion sideband, the muon sideband, and the neutrino high energy sideband. Finally, in Appendix C the reader can find the open data plots for this study as well as the correlation matrices used in uncertainty calculations.

Chapter 2

Neutrinos

The purpose of this chapter is to give the reader a working background knowledge of neutrinos. This chapter will also serve as an introduction to MiniBooNE's Low-Energy Excess, of which the reader will find a more in-depth discussion in chapter 3.3.

2.1 Neutrinos: A Small History

Here a brief historical background of the neutrino is presented. Further information can be found in the citations, as well as numerous books on the subject.

The neutrino (Italian for "little neutral one") was originally conceived of by Wolfgang Pauli in 1930 as an answer to a mathematical discrepancy in beta nuclear decays, namely that the electrons were emitted with a spectrum of energies that never added up to the original amount. This violates energy conservation, one of the fundamental laws of physics: energy can neither be created or destroyed, only changed from one form to another. Therefore, Pauli postulated, some particle had to be missing from the equation that accounted for the "missing" energy from a beta decay, and was also electrically neutral. Additionally, it needed to have an incredibly small mass and an angular momentum spin of $\frac{1}{2}$. While this was fiercely debated amongst physicists at the time, Pauli would later be proven correct.[2]

Neutrinos cannot be directly observed due their electrically neutral nature, but the byproducts of their interactions can be. If a neutrino strikes a neutron, it can produce a proton and an electron:[2]

$$\nu_e + n^0 \longrightarrow p^+ + e^-$$

The neutrino interacts with matter only via the Weak Nuclear Force, meaning it has to interact directly with the nucleus of an atom. Due to atoms being mostly empty space, this has produced the well-known axiom: "a neutrino can pass through a light year's worth of lead without producing a single interaction". In 1956 the first indirect evidence of the neutrino was observed by Fred Reines and Clyde Cowan Jr. in an experiment at the Omega West Reactor at Los Alamos National Laboratory. This observation was of the anti-neutrino variety:

$$\bar{\nu}_e + p^+ \longrightarrow n^0 + e^+$$

Due to the highly classified nature of nuclear reactors at the time, it would be 8 years before their findings were independently verified.[2]

A further point was discovered later that there were other "types" of electrons; this group of particles is now referred to as leptons. The muon (μ) was discovered in the mid-1950s, and the tau (τ) was discovered in the mid-1970s. Neutrinos have types as well, now called "flavors", that pair with each lepton: the electron neutrino (ν_e), the muon neutrino (ν_μ), and the tau neutrino (ν_τ). The neutrino oscillates between all three flavors; never fully any one until measured.[2]

2.2 A Neutrino Conundrum

2.2.1 Then ...

From 1993 to 1998, Los Alamos National Laboratory ran an experiment called LSND (Liquid Scintillator Neutrino Detector). It was designed to detect the appearance of electron anti-neutrinos using a proton beam hitting a target and then generating a nearly pure beam of muon anti-neutrinos. After 30 meters some of the muon anti-neutrinos would have oscillated into electron anti-neutrinos, hit the detector and interacted with the protons within. This would produce electrons and neutrons within the detector. The trouble was that more electron anti-neutrinos were found than other experiments and theory had suggested. The discrepancy was such that another experiment was run to double-check the results: MiniBooNE.

MiniBooNE was designed to be much larger than LSND (approximately 10 times larger) and sensitive to the signal seen by LSND, but was a different type of detector. Also an appearance detector, MiniBooNE could detect both the electron neutrino and its anti-neutrino counterpart. This would allow any contributions that LSND may have made to be ruled out. Running from 2002 through 2019, expectations were that MiniBooNE would refute the results of LSND. Instead, MiniBooNE found its own excess in the low energy range, referred to as the Low-Energy Excess (LEE). More specifics about the MiniBooNE detector and the LEE is discussed in Chapter 3.[2]

2.2.2 ... And Now

A third experiment was then conceived. MicroBooNE ran from 2015 through 2021, and is a better detector than MiniBooNE for resolving individual particle tracks and differentiating electrons from other particles.[3] MicroBooNE began releasing results related to searches for the low-energy excess in 2022. Thus far, nothing has been found to corroborate either of the excesses seen in MiniBooNE or LSND.[4–8] One one paper has suggested an area of further exploration, having found a modest 2.2σ excess in the correct region.[9;10] Further discussion occurs in Chapter 4.

Chapter 3

The MiniBooNE Experiment

The purpose of this chapter is to give an overview of the MiniBooNE detector, particularly the parts relevant for this study. This includes the general location and size of the detector, the PMTs, and information about the mineral oil it was filled with. This chapter also includes theoretical background on the physics of Cherenkov radiation, which was vitally important to the MiniBooNE detector and this study. The chapter concludes with a discussion of MiniBooNE's Low-Energy Excess result.

3.1 The MiniBooNE Detector

3.1.1 MiniBooNE at Fermilab

The MiniBooNE detector was designed and developed as a scintillation and Cherenkov light detector for detecting neutrino oscillations, specifically muon neutrinos to electron neutrinos. MiniBooNE's spherical tank had a diameter of 12.2 meters, and was located in a 13.7 meter diameter cylindrical vault underground at Fermi National Accelerator Laboratory (Fermilab). It was then further covered by another 3 meters of dirt. The detector utilized the Booster Neutrino Beam (BNB), which is produced by 8 GeV protons that have been extracted from the Fermilab Booster synchrotron and have then interacted with a beryllium target located 541 meters away from the detector. This interaction produces pions and kaons that decay to neutrinos while traveling down a 50 meter decay pipe. The BNB has a mean energy of 500 MeV and two modes: a neutrino mode and an anti-neutrino mode. The respective flux contributions at the MiniBooNE detector were 93.5% ν_μ, 5.9% $\bar{\nu}_\mu$, 0.5% ν_e, 0.1% $\bar{\nu}_e$ and 15.7% ν_μ, 83.7% $\bar{\nu}_\mu$, 0.2% ν_e, 0.4% $\bar{\nu}_e$. The MiniBooNE detector collected data from 2002-2019, with a total of 18.75×10^{20} protons-on-target (POT) in neutrino mode and 11.27×10^{20} POT in anti-neutrino mode.[11;12] An aerial view of MiniBooNE's location in relation to MicroBooNE and the BNB can be seen in figure 4.1.

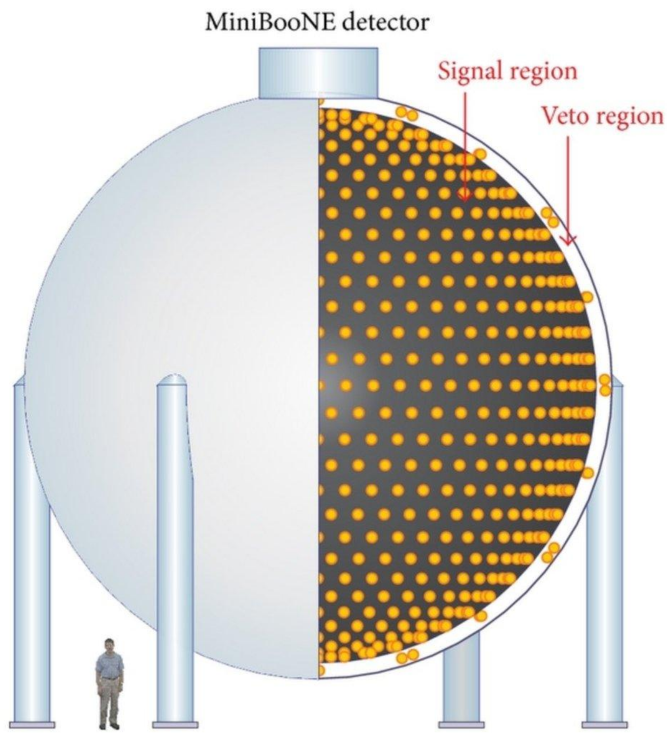

Figure 3.1: A cut-away drawing of the inside of the MiniBooNE tank showing the 1520 PMTs within made up of two layers: the signal region layer consisting of 1280 PMTs facing inward to detect Cherenkov and scintillation light, and the veto region layer made of the remaining 240 PMTs that faces outward to detect light caused by cosmic ray showers.[11]

3.1.2 MiniBooNE's Cherenkov and Scintillation Tank

MiniBooNE's internal surface had a total of 1520 PMTs installed (Figure 3.1). A total of 1198 PMTs were reused from the Liquid Scintillator Neutrino Detector from the Los Alamos National Laboratory. Of the 1520 PMTs, 1280 were used for the signal region and

240 were used for the veto region. The signal region PMTs facing inside the tank detected the Cherenkov and scintillation light produced when charged particles at the correct energies interacted with the mineral oil. The veto region layer of PMTs, still mounted inside the tank, faced outward to detect signals caused by cosmic ray showers and were optically isolated from the signal region. The maximum wavelength-dependent efficiency occurred at 390 nm. They were operated at a positive voltage of approximately 2000 V, and had a gain of approximately 1.6×10^7.[11] The PMTs and an intrinsic charge resolution of approximately 15% at 1 *p.e.*, and an intrinsic time resolution of approximately one nanosecond. The layout of the PMTs on the internal surface had a light leakage of less than 10^{-3} (Figure 3.2).[11;12]

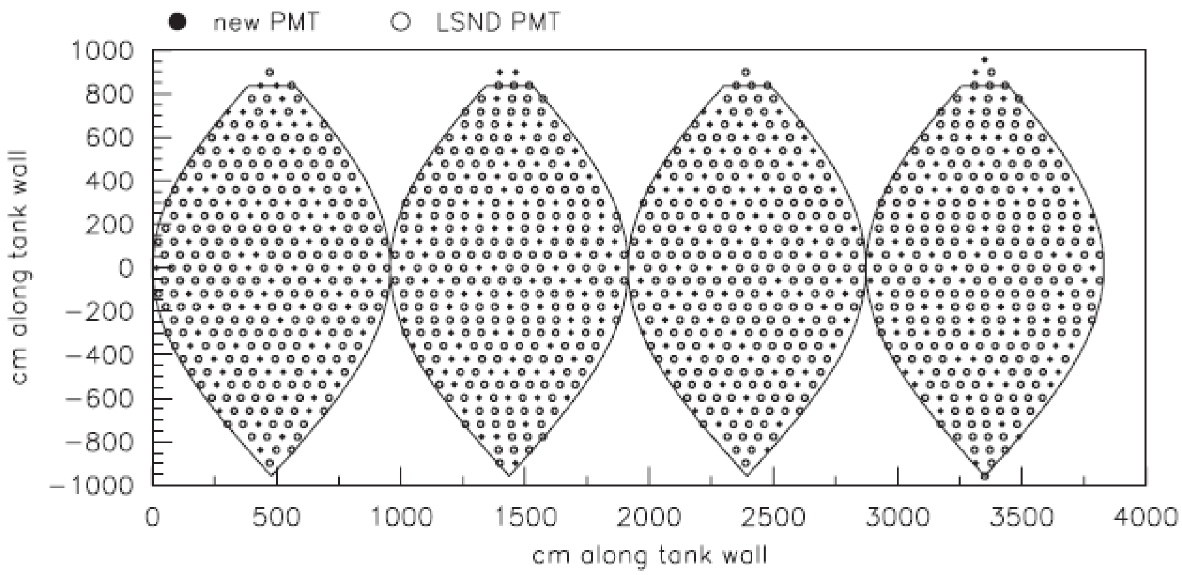

Figure 3.2: MiniBooNE's photo-multiplier tube layout.[11]

MiniBooNE was filled with 818 tons (approximately 9.5×10^5 liters) of Marcol 7 light mineral oil (CH_2), with an exact index of refraction

$$n = (1.4684 \pm 0.0002) \times [1 - (3.66 \pm 0.04) \times 10^{-4} (T - 20\ ^\circ C)] \tag{3.1}$$

and an effective index of refraction of $n = 1.4620$. MiniBooNE used the naturally occurring scintillation light present in pure mineral oil to help identify certain processes that produce additional slow-moving hadronic particles. The extinction length used in MiniBooNE's light extinction function used for modeling and simulation is approximately 40 meters at 460 nm.[11;12]

3.2 Cherenkov Radiation in MiniBooNE

This study necessitates a discussion of Cherenkov radiation and the mathematics behind it. Cherenkov radiation is the name given to radiation that occurs when the velocity of a particle traveling through a transparent medium is greater than the speed of light traveling through that same medium, regardless of whether the transparent medium is solid, liquid, or gas.[13] The speed of light in the transparent medium is defined as:

$$c = nv$$

where v is the velocity of light in the medium, n is the index of refraction of the transparent medium, c is the velocity of light in a vacuum. While the highpoint is in the visible spectrum of light at approximately 420 nm, Cherenkov radiation contains a continual spectrum of wavelengths that extends from the visible region to the near-UV region of light. Photon emissions found in the microwave to infrared regions of light are insignificant.

Cherenkov radiation is emitted when polarized molecules in the medium return to their original states. The radiation is emitted asymmetrically in the direction of the particle trajectory at an angle relative to the particle track. The angle θ is a function of the particle's phase velocity and the index of refraction of the transparent medium. This is usually depicted in 2-D as a conical wave front (Figure 3.3), and a cross section taken perpendicular to the wave front shows the radiation taking the form of concentric rings (Figure 3.4).[13]

Cherenkov radiation can only occur above the radiation threshold in the transparent medium given by

$$\beta n \;=\; 1$$

where β is the velocity of the particle relative to the speed of light ($\beta \;=\; \frac{v}{c}$) and n is the

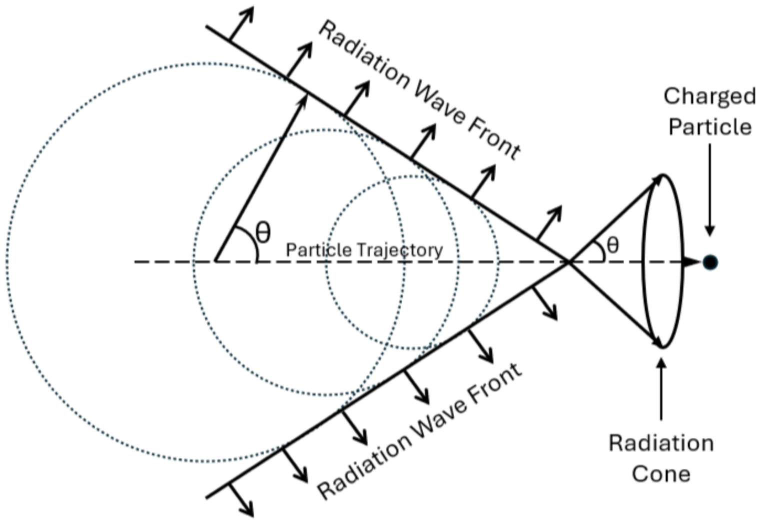

Figure 3.3: A 2-D depiction of the conical wave fronts of Cherenkov radiation.[13]

index of refraction of the transparent medium. Charged particles that exceed this velocity ($\beta > \frac{1}{n}$) will produce Cherenkov radiation in a transparent medium.[13] This can be further solved for the "critical velocity" that charged particles must exceed to produce Cherenkov radiation in MiniBooNE, and is used for this study:

$$v_{crit} > \frac{c}{n}$$

The value of β is dependent on its kinetic energy, therefore it is also dependent on the rest mass of the charged particle:

$$E = m_0 c^2 \, [\frac{1}{(1-\beta^2)^{1/2}} - 1]$$

where m_0 is the rest mass of the particle, c is the velocity of light, and E is the kinetic energy. This is known as the threshold energy for a charged particle to produce Cherenkov

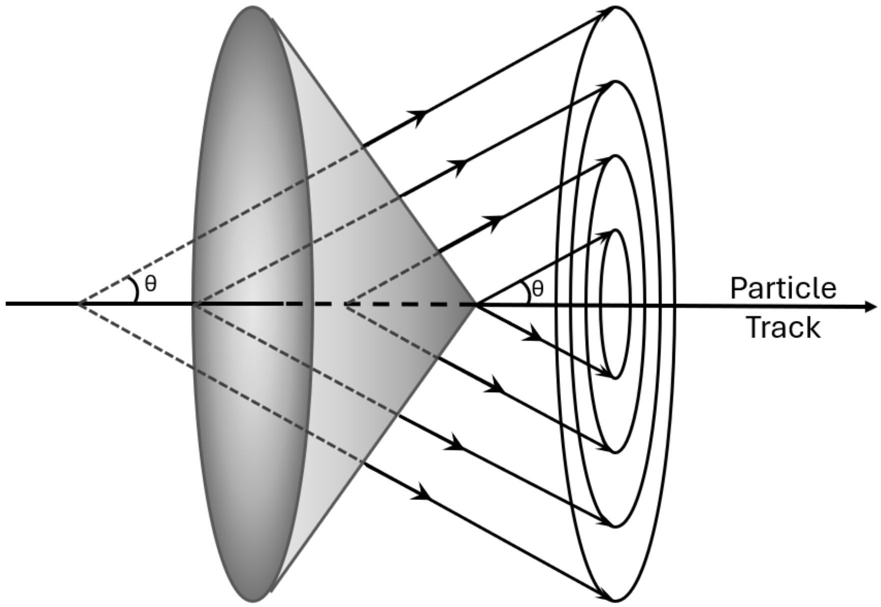

Figure 3.4: A 3-D depiction of the conical wave fronts of Cherenkov radiation with the cross section of concentric rings along the particle path shown.[13]

radiation:

$$E_{th} \; > \; m_0c^2 \; [(1 \; - \; \frac{1}{n^2})^{(-\frac{1}{2})} \; - \; 1]$$

An important note to make is that the energy threshold for a charged particle to produce Cherenkov radiation will vary according to the particle's rest mass and the index of refraction of the transparent medium. A higher index of refraction will lower the energy threshold, while conversely a higher particle rest mass will increase the energy threshold.[13]

Because the effective index of refraction for the transparent medium within the MiniBooNE detector (Marcol 7 mineral oil, see Chapter 3.1.1) is nearly constant, the energy threshold (and therefore the velocity threshold) for MiniBooNE was solely dependent upon the rest mass of the particles interacting with the mineral oil. Further discussion on how this is used in this study can be found in Chapter 5.

3.3 The Low-Energy Excess

MiniBooNE's purpose as an experiment was to explore an interesting excess seen by the LSND experiment at Los Alamos Nation Laboratory. Further discussion of those results are neither feasible nor necessary to the discussion at hand, but the interested reader may look to the citations of Chapter 2 for more information. Suffice to say, MiniBooNE found no evidence of LSND's excess, but instead found one of their own.[1]

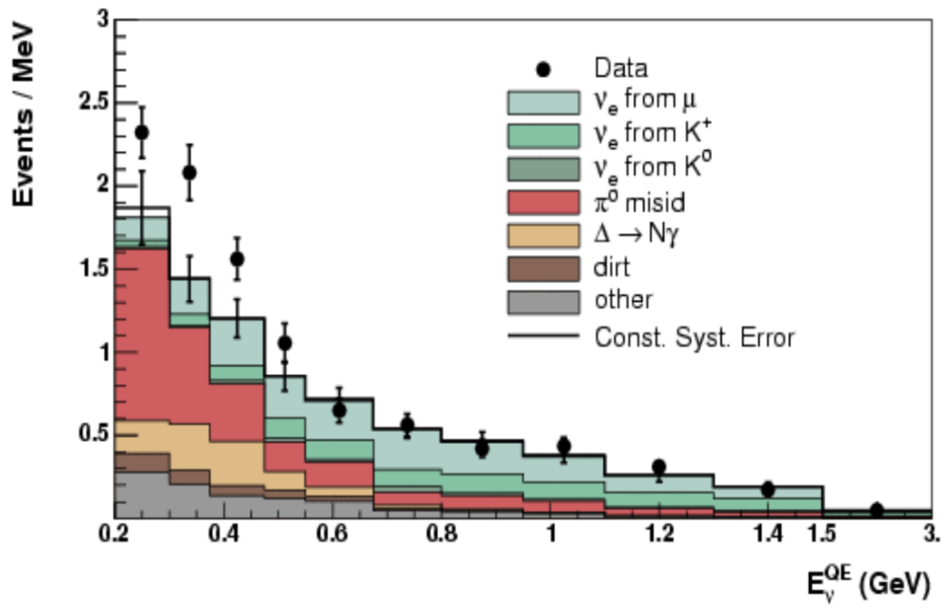

Figure 3.5: The original low-energy excess from MiniBooNE's 2018 paper showing an excess of 4.8σ.[1]

Located in the 200-475 MeV range, the MiniBooNE low-energy excess presents an interesting topology seen in figures 3.5 and 3.6. The largest background presented here is misidentified neutral pions. These particles typically decay to two photons[14]

$$\pi^0 \longrightarrow \gamma\gamma$$

which appear as two showers in a Cherenkov detector when both showers are fully contained within the detector, but may appear as only one shower if one of the photons is not detected. This background is quite high, and is identified as "π^0 misid" (mis-identified pions, dark pink)

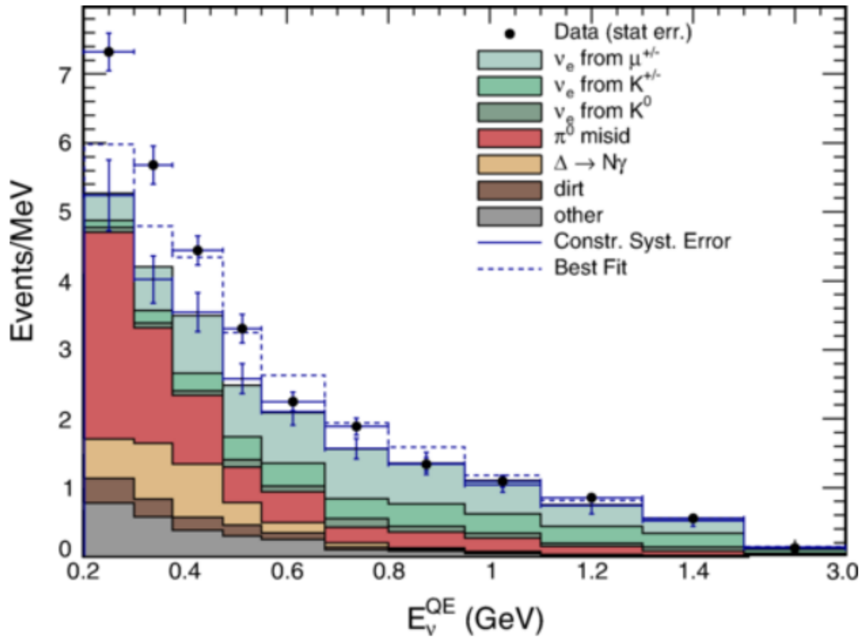

Figure 3.6: The most recent low-energy excess from MiniBooNE's 2021 paper showing an excess of 4.9σ.[12]

in figures 3.5 and 3.6. The MiniBooNE detector had great difficulty distinguishing between a single shower produced by an electron and a single shower produced by a photon.[11]

Chapter 4

The MicroBooNE Experiment

One of the main purposes of the MicroBooNE (Micro Booster Neutrino Experiment) is to determine the nature of the MiniBooNE Low-Energy Excess.[3] Many analyses have been conducted by the MicroBooNE Collaboration in pursuit of this goal; an overview of the results of these analyses is given in Chapter 3.3. This chapter gives an overview of the parts of the MicroBooNE detector relevant to this study (chapter 4.1), and concludes with a discussion of MicroBooNE's low-energy excess results so far (chapter 4.2.

4.1 The MicroBooNE Detector

4.1.1 MicroBooNE at Fermilab

Unlike the underground MiniBooNE detector, the MicroBooNE detector is a surface-level Liquid Argon Time Projection Chamber (LArTPC) detector located at Fermi National Accelerator Laboratory (Fermilab). Operations ran from the fall of 2015 through the summer of 2021, and collected 1.3×10^{21} POT from the BNB for the full data set. MicroBooNE is installed 470 meters on-axis from the beryllium neutrino production target of Fermilab's BNB. An aerial view of MicroBooNE's location in relation to MiniBooNE and the BNB can be seen in figure 4.1.[3] Further discussion about Fermilab's BNB can be found in Chapter 3.1.1.

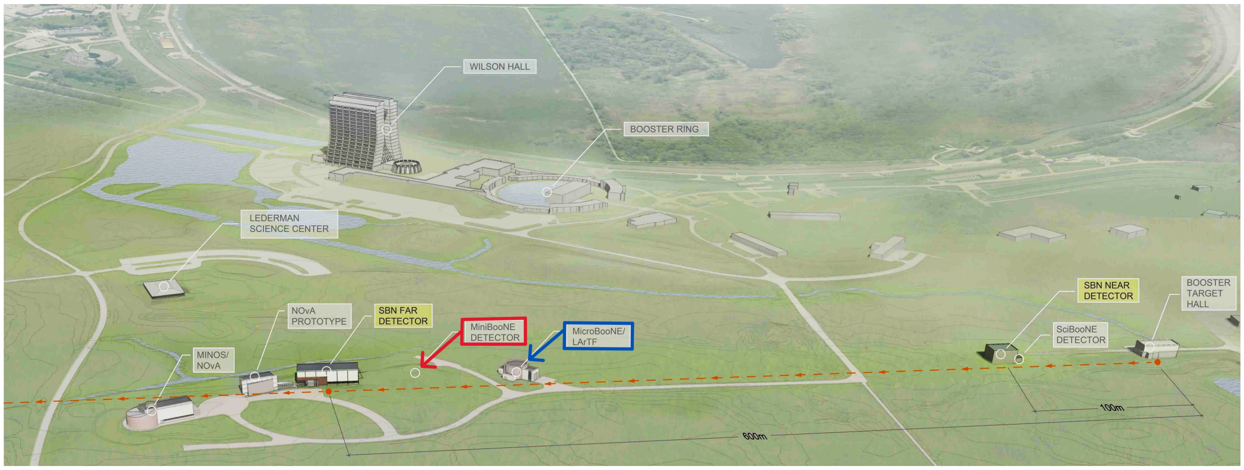

Figure 4.1: Aerial drawing of Fermilab showing the location of MiniBooNE (red), MicroBooNE (blue), and the path of the booster neutrino beam (orange dashed line).[3]

Additionally, MicroBooNE is off-axis by 8° and is located approximately 600 meters from Fermilab's Neutrinos at the Main Injector (NuMI) beam neutrino production target.[3] The NuMI beam is produced from 120 GeV protons that have been extracted from the Fermilab main Injector. After the protons are extracted, they travel 350 meters towards the NuMI graphite target. The interaction with the target produces primarily charged pions and kaons, which will then be directed by two magnetic horns to travel 675 meters down a decay pipe. The pions and kaons both decay to muon neutrinos, producing a ν_μ beam similar to the BNB.[15] NuMI has an average energy of 250 MeV from pion decay and 2 GeV from kaon decay at MicroBooNE's 8° off-axis angle.[16]

MicroBooNE also utilizes a 32 PMT light detection system, with a timing resolution on the order of microseconds. A cosmic-ray tagger (CRT) is also employed by MicroBooNE. As a surface-level detector, MicroBooNE's largest background to neutrino interactions are cosmic rays. Combined, these two tools allow rejection of the cosmic ray background during data processing with precise spatial and timing information.[4;15]

4.1.2 Liquid Argon Time Projection Chamber

An overview of MicroBooNE's LArTPC is presented here. Further specificity can be found in the cited MicroBooNE paper and the citations therein. The MicroBooNE LArTPC, as the name would suggest, is filled with highly purified liquid argon (85 tonnes). Charged particles interact with the argon, ionizing it while leaving trails of ionization electrons. MicroBooNE's LArTPC is composed of three major components. The first major component is the three anode planes and the cathode plane. The cathode's voltage ran at $-70\ kV$, which produces a uniform electric field between the cathode and anodes with a measured drift-field of 273 V/cm.[4;15]

The second major component is the three wire planes, of which a concept drawing can be seen in figure 4.2. Two induction planes (referred to by MicroBooNE as the "U" and "V" planes) have their wires oriented at $\pm 60°$ with respect to vertical. The bias voltage for the U plane is $-110\ V$ and $0\ V$ for the V plane. The third is a collection plane (referred to by MicroBooNE as the "Y" plane) with a bias voltage of $+230\ V$ and wires oriented vertically. The ionized electrons drift towards the three wire planes to yield three different two-dimensional views of a potential neutrino interaction. The maximum drift time, from the cathode to the U plane is 2.2 ms. Combined with the three wire planes that were spaced only 3 millimeters apart, this creates a three-dimensional reconstruction of these interactions on millimeter scale spatial resolution.[4;15] These reconstructed images are accomplished using the Pandora reconstruction framework (see Chapter 4.1.3).[17]

The last component is the surrounding field cage to create the uniform electric field needed for a constant drift-field by enclosing the volume between the cathode plane and the anode wire planes. This is referred to as the "active" volume, defined by the field cage interior and bounded by the cathode and anode planes. It also helps protect the outside sensitive electronics from the high voltage of the cathode. This entire structure is enclosed within the cylindrical cryostat to keep the liquid argon at the correct temperature and prevent the argon from boiling. This can be seen in figure 4.3.[3]

4.1.3 The Pandora Reconstruction Framework

MicroBooNE utilizes the Pandora reconstruction framework to process the raw space-charge point data that comes from the wire planes into usable data. The constant electric field

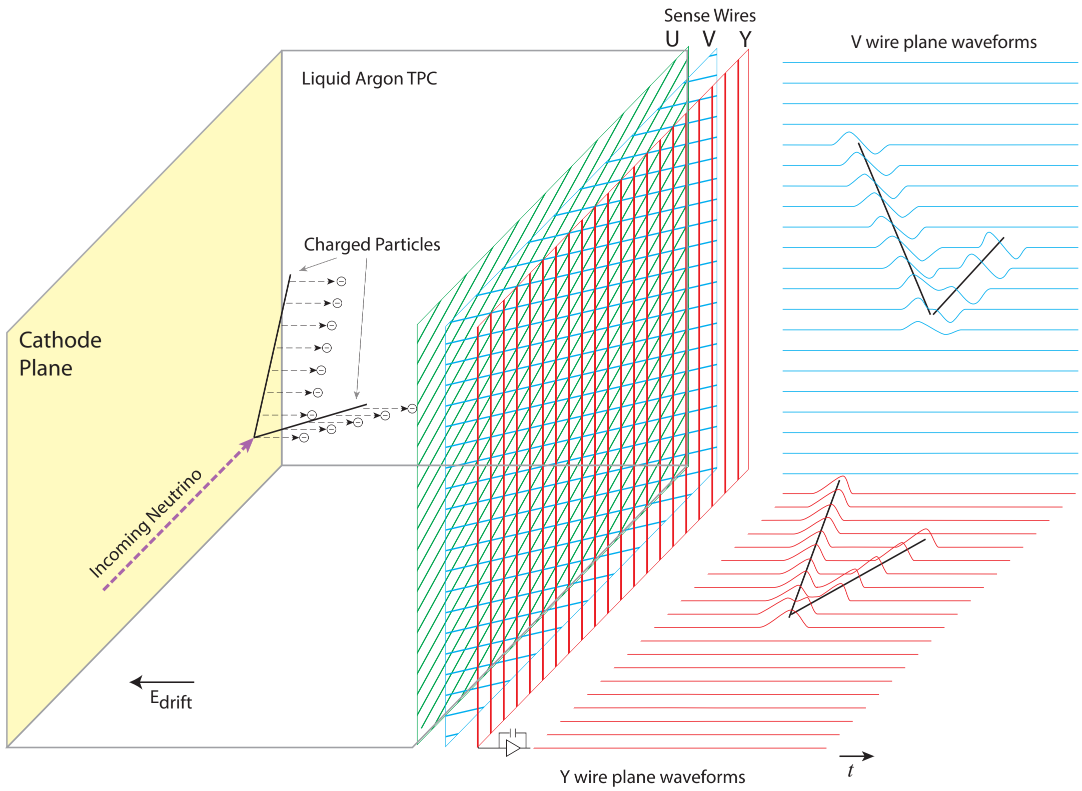

Figure 4.2: Concept drawing of the functionality of MicroBooNE's LArTPC wire planes.[3]

creates a known drift velocity, therefore charge from a particle is deposited in a particle order that gives length and direction of travel. When a charged particle drifts toward the wire planes, it deposits charge along a series of wires at specific times. Pandora then reconstructs these hits into a track or shower, given various parameters such as vertex location and length and spread of the deposited charge. Pandora groups features near to each other into "slices" containing possible interaction features. More information on how MicroBooNE uses Pandora can be found in the cited paper.[17]

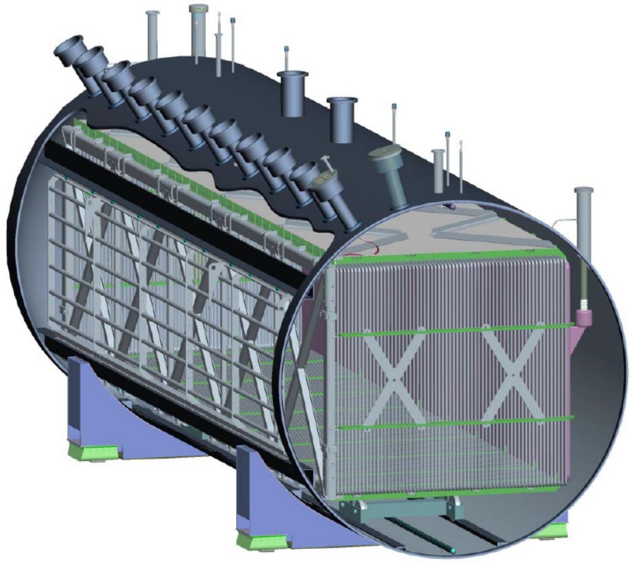

Figure 4.3: Schematic diagram of the MicroBooNE LArTPC situated within the cryostat from the "Design and Construction of the MicroBooNE Detector" paper.[3]

4.2 MicroBooNE's Low-Energy Excess Results So Far

MicroBooNE has looked exhaustively for MiniBooNE's low-energy excess and has found no evidence of it, save for one paper.[9] MicroBooNE's first round of low-energy excess results included a look neutrino-induced neutral current delta radiative decay, charged current quasi-elastic electron neutrino interactions, charged current electron neutrino interactions without pions, and electron neutrino interactions using multiple final state topologies, all without any evidence of an excess.[4–8] Later results looked at the possibility of light sterile neutrinos, more inclusive (multi-channel) examinations of charged current electron neutrino interactions, and further searched involving neutral current delta radiative decay to a single photon. Again, all found no evidence of an excess.[18–20] The only hint of an excess comes from the inclusive (all channels) examination of single photon events. However, at only 2.2σ, it is nowhere near statistically significant enough to make any sort of claim of discovery. It does encourage a further examination though since this result only utilizes the first three runs of MicroBooNE data, which amounts to just over half the total data now available.[9]

Chapter 5

Methods of this Study

The purpose of this chapter is to provide an overview of the PeLEE framework that was used for this study, as well as the signal definition and specific selections used. The methodology involves using ntuples produced using the Pandora reconstruction framework.[4] These ntuples are fed into a program written using a combination of Python and C++ that instructs ROOT[21] to read the ntuples to look for showers. These will be checked if they produced Cherenkov radiation (see 5.2.2), and if so, will be used in this study.

MiniBooNE was unable to record interactions that occurred below the Cherenkov radiation threshold (see Chapter 3.2 on Cherenkov radiation, approximately 200 MeV), with an exception for tracks that began above the energy threshold but ended below the visible range. The invisible portion could be extrapolated from the visible portion recorded by the MiniBooNE detector. Therefore, various interactions and their rates of occurrence (cross sections) had to be modeled.[22] However, MicroBooNE has a much lower limit of sensitivity (approximately 40 MeV).[4] First, MicroBooNE's truth Monte Carlo and reconstructed Monte Carlo is compared to MiniBooNE's modeling using the PeLEE code framework. Any discrepancies between MiniBooNE's modeling and MicroBooNE's modeling have been identified and adjusted for. The final study will examine the open data from MicroBooNE and modeling from MiniBooNE, and attempt to determine if the LEE can be reproduced using MiniBooNE's modeling and MicroBooNE data. By doing this, if the excess is reproduced, it may be possible to identify the particle makeup of the Low-Energy Excess seen by MiniBooNE.

5.1 The PeLEE Framework

The PeLEE code framework and corresponding ntuples were used to conduct this study. An overview is presented in this section; further details can be found in the cited papers. The PeLEE framework was designed and implemented to search for an excess of electron neutrino (ν_e) events over the predicted BNB intrinsic interaction rate. It uses the BNB neutrino flux simulation originally developed by MiniBooNE, but adjusted for MicroBooNE's detector location for the flux model.[4] The neutrino interaction modeling is done using the GENIE event generator, specifically GENIE v3.0.6 G18_10a_02_11a.[23] This allows for the simulation of neutrino interactions within MicroBooNE, and also models the outgoing final-state particles produced by these interactions. Geant4 v10_3_03c[24] and LArSoft[25] are used to model the detector by simulating the propagation of particles and the propagation of light and charge through the detector, respectively.[4]

The PeLEE ntuples were created to be used with the PeLEE framework using the Pandora reconstruction framework (see Chapter 4.1.3), and utilize a subset of 1.1×10^{21} POT for the Monte Carlo. A note that ntuples are commonly used in high energy physics for storing many variables of differing lengths. These variables can be scalars or vectors. The PeLEE ntuples contain most of the variables necessary to conduct this study. Some variables were created and calculated from variables in the PeLEE ntuples. These will be listed in the following section in Table 5.1.

5.2 Signal Selection

The signal for this study is defined as a shower-like event that would have generated Cherenkov radiation if had been detected by a MiniBooNE-like detector, without any other associated Cherenkov-visible showers or tracks. Therefore, a single Cherenkov-visible shower is required to be present while no Cherenkov-visible muon tracks must be present:

$$\nu \longrightarrow 1\ Shower^{vis} + 0\ \mu^{vis}$$

To this end, two sets of code are used to generate the plots within the PeLEE framework. The first set of code is the “construction” code; this code does most of the heavy-lifting in terms of calculations and creating the needed variables for this study. The first set of selections are applied in this code to create the signal definition. The second set is the plotting code. This is lighter-weight code that is not calculation-heavy, and is where the background-reduction selections take place. This is also the set of code that was used to conduct uncertainty testing, which will be further elaborated on in Chapter 6.3.

5.2.1 Background and Plot Legend Definitions

The background to the selected signal is defined to be non-signal events, however it is helpful to the reader to further define it here in context of the plots presented in this study. The reader will notice in the legends a white, diagonal-lined option labeled “EXT”. These are events that occur external to the neutrino beamline, and then are recorded by the MicroBooNE detector. Because they do not originate from the beamline, they are always considered background events.

Additionally, the reader will see a dark red option labeled “Out. fid. vol.” (out of fiducial volume). These are events that originated from the neutrino beamline, but the vertex of the event occurs outside of the MicroBooNE detector fiducial volume (defined as a rectangular prism within the MicroBooNE detector that allows for the best event record). Out of fiducial volume events are usually poorly reconstructed due to a missing vertex, and are also always considered background events.

Further background for the selected signal will come from neutral pions (π^0), which are seen decaying through neutral-current interactions from any neutrino (labeled ν NC π^0, light blue) and specifically from muon neutrinos through charged-current interactions (labeled ν

CC π^0, medium blue). Some of the muon neutrino events (cyan) will also be background, but not all (see Chapter 5.3.2).

Finally, the reader will notice in the legends events labeled ν NC in dark blue. These are events that originate from neutral-current neutrino interactions. In various shades of green are the different events orginating from electron neutrinos including charged-current events with zero pions and any number of protons (ν_e CC0πNp), charged-current events with zero pions and zero protons (ν_e CC0π0p), and other charged-current events (ν_e CC). The black line is the total predicated number of events from Monte Carlo and external events, and the transparent gray indicates the uncertainty. The red-dashed line is PeLEE's model of the MiniBooNE low-energy excess, and it indicates the number of additional events needed if a MiniBooNE-like excess were to appear in MicroBooNE's data.[4] Ideally, after all background reductions and selections are applied, the red-dashed line will be higher than the black line and outside of the transparent gray area.

5.2.2 Shower Selection

A variable was created using the PeLEE frameworks that checks how many showers in a slice (interaction) would have produced Cherenkov light in a MiniBooNE-like detector (*nshr_visible*). It takes the corrected shower energy variables for the first, second, and third showers and compares them to the cutoff that MiniBooNE used for visible showers (100 MeV).[1]

A further selection was created to force the code to treat two showers as one shower if the vertex and angular distance between the two showers was below MiniBooNE's vertex and angular resolutions.[1] This is equal to less than 20 cm distance between the two vertices (*shr12_dx*). The angular resolution is less than 13° angular separation, the cosine of which is: $cos(13°) \approx 0.9743$ (*pi0_gammadot*). This is then used to determine a new variable (*nshr_mB_vis*) that counts the number of Cherenkov-visible showers after any colinear recombination of showers is done. This is summarized in Table 5.2.

Table 5.1: List of variables used from PeLEE ntuples, variables created by the PeLEE framework, and variables created from PeLEE ntuple variables for this study.

PeLEE ntuple Variables	Variables Created by PeLEE Framework	Variables Created by this Study
shr_energy_cali	shr12_start_dx	nshr_visible
shr_energy_second_cali	shr12_start_dy	nshr_mB_vis
shr_energy_third_cali	shr12_start_dz	corr_shr_energy_cali
shr_pz		corr_shr_energy_second_cali
shr_second_pz		corr_shr_energy_third_cali
shr_score		recoEvQEle
shr_theta		shr12_dx
trk_energy_muon		corr_shr_pz
pi0_gammadot		recoEvQElu

Table 5.2: List of selections implemented to match desired signal (one cherenkov-visible shower plus zero Cherenkov-visible tracks).

Calculation Selection	Variable	Value
Creates Cherenkov Radiation	E_mB_shr_cut	> 0.10 GeV
Force treatment of Two showers as One		
MiniBooNE Shower Vertex Resolution	shr12_dx	< 20 cm
MiniBooNE Shower Angular Resolution	pi0_gammadot	> 0.9743
Use only one shower (including 2 in 1)	nshr_mB_vis	$= 1$

These are all then used to calculate the electron Quasi-Elastic neutrino energy ($E^{QE}_{\nu_e}$):

$$E^{QE}_{\nu e} = \frac{E_{sh} \cdot (M_n - E_B) \ + \ \frac{1}{2}(M_p^2 - (M_n - E_B)^2 - M_e^2)}{(M_n - E_B) \ + \ p_z \ - \ E_{sh}}$$

where E_{sh} is the shower energy, M_n is the mass of the neutron, M_p is the mass of the proton, M_e is the mass of the electron, E_B is the binding energy, and p_z is the shower momentum in the z-direction. This results in figure 5.1.

Additionally, the PeLEE NUE pre-selection was applied to reduce out-of-fiducial volume and external events. These are event that are not fully contained within the detector and generally won't contribute to the measurements done here. The PeLEE NUE pre-selection involves rejecting cosmic events, requiring events to be fully contained within the fiducial

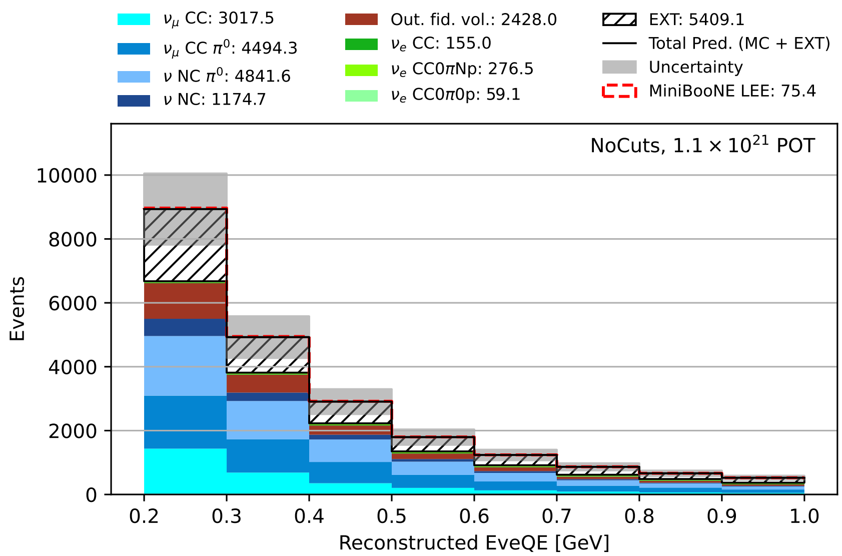

Figure 5.1: Signal region of reconstructed quasi-elastic neutrino energy with no pre-selection or selections applied.

volume, rejecting Michel electrons, and requiring good data quality. This results in figure 5.2, and shows only a slight reduction in out-of-fiducial-volume events.

5.3 Optimal Electron Neutrino MiniBooNE Selection

The purpose of these selections are to mimic MiniBooNE's selections and backgound reductions as closely as possible. Further selections were needed to reduce the background, as well as add in weights for the different Monte Carlo sets. MicroBooNE has four: "mc" refers to the Monte Carlo events that are generated by GENIE, "drt" refers to "dirt events" that are external background events from the beam, "nue" are the ν_e intrinsic from the beam, and "ext" are external background events not from the beam.

As seen in table 5.3, there were four selections made to optimize the number of ν_e interactions and to match MiniBooNE's selections as closely as possible.

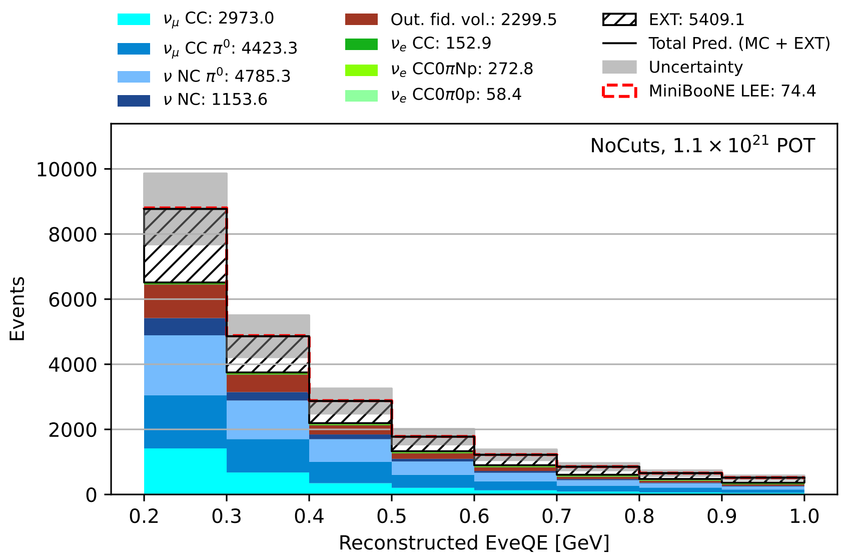

Figure 5.2: Signal region of reconstructed quasi-elastic neutrino energy with only the NUE pre-selection applied.

5.3.1 Selection 1: Only One Cherenkov-Visible Shower

The first selection selected only single Cherenkov-visible showers, while also allowing for any two-shower slices that MiniBooNE might have treated as one shower ($nshr\_mB\_vis$). It can be seen in figure 5.3 and in the plots in Appendix A that this results in a small reduction of out-of-fiducial-volume and EXT events.

5.3.2 Selection 2: Remove Cherenkov-Visible Muon Tracks

The second selection was to remove Cherenkov-visible muon tracks that a MiniBooNE-like detector would have easily differentiated from showers. The threshold for a muon to create Cherenkov radiation in the mineral oil that MiniBooNE used (see Chapter 3.1.2) is approximately 40 MeV of kinetic energy:

$$KE_{crit} = \frac{m_\mu}{\sqrt{1 - {\beta_{crit}}^2}} - m_\mu$$

Table 5.3: List of selections for this study.

Selection	Criteria	Variable Value
NUE Pre-Selection 1	Cosmic rejection	nslice = 1
NUE Pre-Selection 2	Containment	selected = 1
NUE Pre-Selection 3	Michel electron rejection	shr_energy_tot_cali > 0.07 GeV
NUE Pre-Selection 4	Data quality and type	(_opfilter_pe_beam > 0 and _opfilter_pe_veto < 20) or bnbdata = 1 or extdata = 1
Selection 1	Select only one Cherenkov-visible shower	nshr_mB_vis = 1
Selection 2	Remove Cherenkov-visible muon tracks	trk_energy_muon < 0.1 GeV
Selection 3	Select only Shower-like Events	shr_score ≤ 0.05
Selection 4	Remove π^0 background	pi0_score > 0.55

where $\beta_{crit} = \frac{c}{n}$ and $c = 1$. Plugging in the muon rest mass in MeV yields:

$$KE_{crit} = \frac{105.66}{\sqrt{1 - \frac{1}{n^2}}} - 105.66$$

Using the MiniBooNE mineral oil index of refraction gives $KE_{crit} \approx 40$ MeV. MiniBooNE was able to differentiate muons from showers down to only 100 MeV.[1] Consequently, the selection was made to match MiniBooNE's capabilities.

5.3.3 Selection 3: Select Only Shower-like Events

The third selection selected only shower-like events to further minimize the number of Cherenkov-visible tracks in the signal. The cut-off was selected to be 0.05 on a 0 to 1 scale, where 0 is most shower-like and 1 is most track-like (see Appendix A). This is shown to result in another modest reduction of EXT events and a significant reduction in out-of-fiducial-volume events.

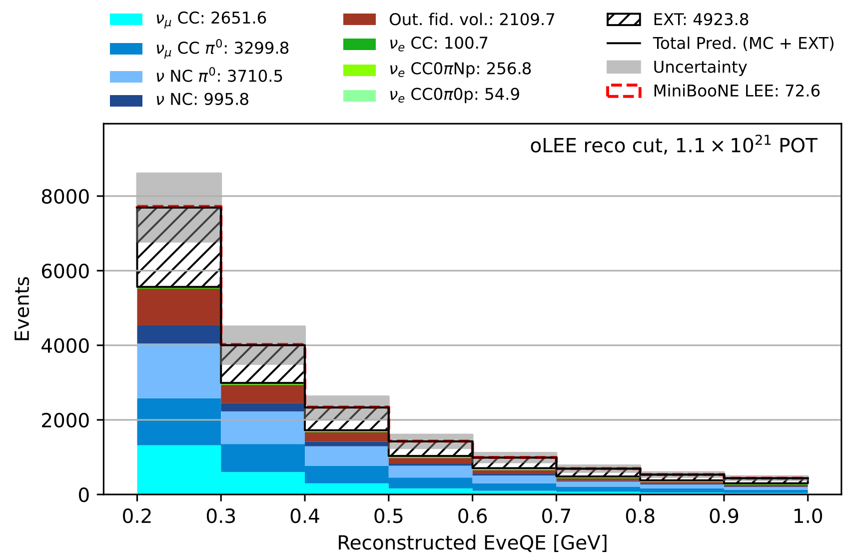

Figure 5.3: Signal region of reconstructed quasi-elastic neutrino energy with the NUE preselection and selection 1 applied.

5.3.4 Selection 4: Remove Neutral Pion Events

The fourth selection removed π^0 events using the likelihood score variable (pi0_score) as an approximation of MiniBooNE's log-likelihood π^0 cut found in the supplemental material of their 2018 paper. This was done by examining MiniBooNe's plots before and after their log-likelihood π^0 cut.[1] The data for the number of mis-identified π^0 events (dark pink) was extracted from these plots, and the corresponding event reduction percentage was found to be approximately 97.7% (see figure 5.6).

Next, PeLEE's *pi0_score* variable was examined with selections 1-3 applied over it's full range. This yielded a total π^0 event count of 3230.2 (see figure B.3a). Applying the event reduction rate gives a target event count of 73 π^0 events. To determine he corresponding *pi0_score* value, several different ranges (see figures B.3 and B.4). The range that was found to give the closest event count was 0.55-1, which gave a total π^0 event count of 74 an under-reduction by less than 1%.

This is shown to result in a significant reduction in all events, particularly background events. Additionally, a difference between the LEE model line and the total prediction is finally seen. Unfortunately, this difference is still well within uncertainty. This can be

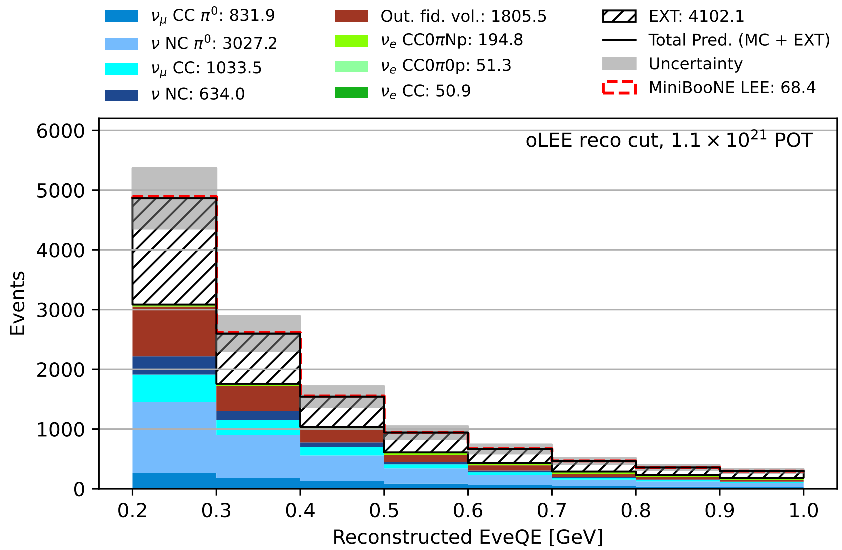

Figure 5.4: Signal region of reconstructed quasi-elastic neutrino energy with the NUE pre-selection and selections 1 and 2 applied.

due to this selection being only an approximation of the corresponding MiniBooNE cut. PeLEE's *pi0_score* variable contains information (specifically the space-charge deposits) that MiniBooNE would not have access to. A better approximation would be to use a different method found in Kelly and Kopp [26], which involves using only the angle between showers and the ratio of the highest energy shower to the total energy of the two showers. This method would not use any information that MiniBooNE did not have. [26] This can be conducted in a future study.

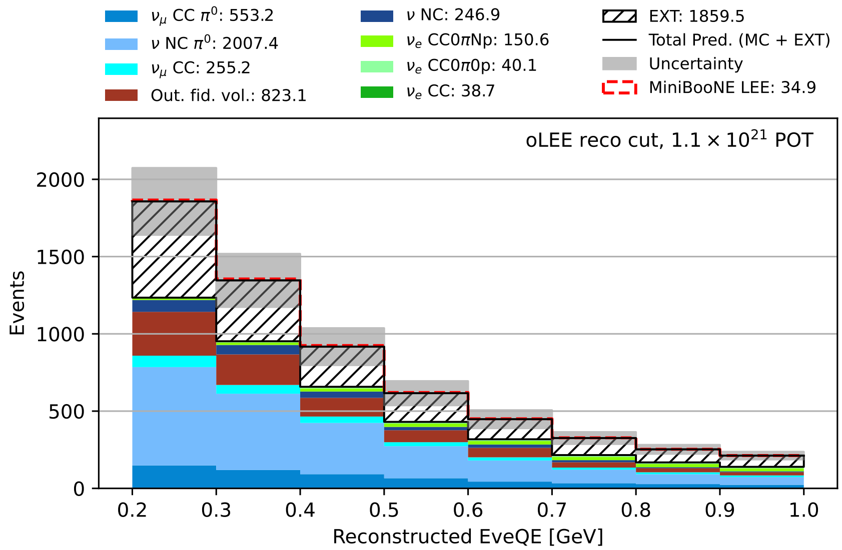

Figure 5.5: Signal region of reconstructed quasi-elastic neutrino energy with the NUE preselection and selections 1, 2, and 3 applied.

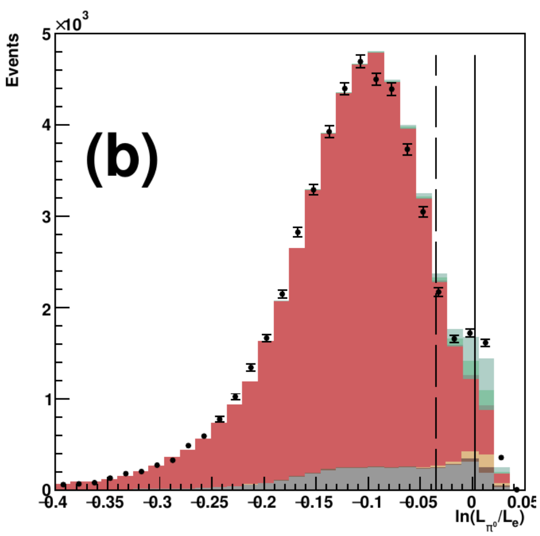

(a) Before MiniBooNE log-likelihood π^0 cut was applied. Total number of mis-identified π^0 events (dark pink) extracted is approximately 46,369.

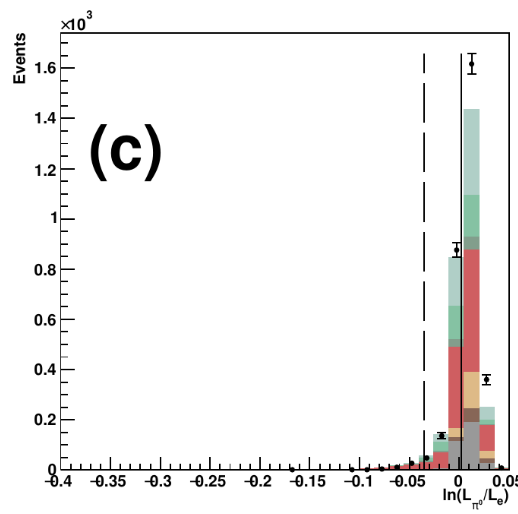

(b) After MiniBooNE log-likelihood π^0 cut was applied. Total number of mis-identified π^0 events (dark pink) extracted is approximately 1,044.

Figure 5.6: Part of figure 13 from MiniBooNE's 2018 paper showing before and after their log-likelihood π^0 cut was applied.[1] This results in an approximate 97.7% reduction of mis-identified π^0 events (dark pink).

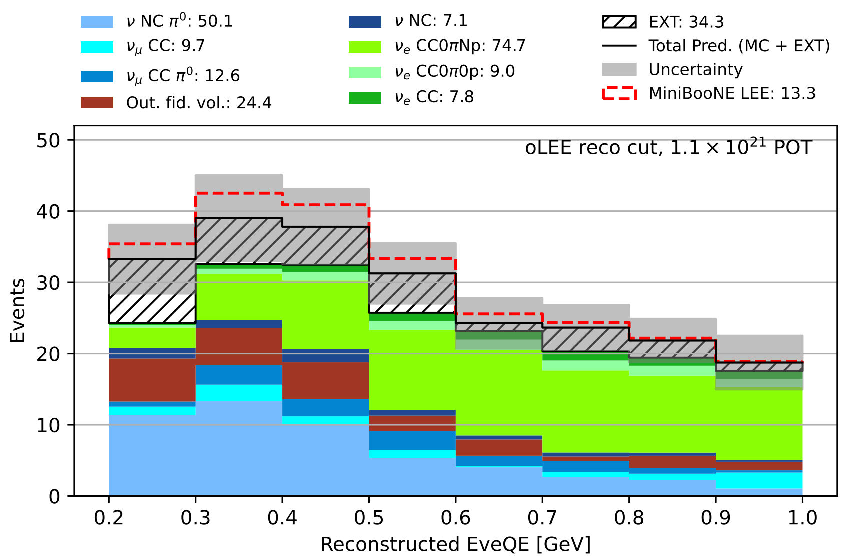

Figure 5.7: Signal region of reconstructed quasi-elastic neutrino energy with the NUE pre-selection and all 4 selections applied.

Chapter 6

Results: Analysis and Discussion

The three sidebands will now be examined. There will be an examination of the π^0 sideband (a known background for MiniBooNE and MicroBooNE), a look at the sideband of quasi-elastic energy of muons in the same energy range as the signal, and the high energy range of the signal (1-3 GeV). These sidebands will be used later to constrain the uncertainty in the signal region. This is done by selecting one or more sidebands that are proven to not fluctuate when changes are made in the signal region. Uncertainties are determined for these sidebands, and tend to be lower than uncertainties in the signal region. These lower uncertainties are then applied to the signal region in order to reduce uncertainties there.

6.1 Sideband Study

As part of the unblinding procedures for MicroBooNE, several sidebands are examined to visualize how various selections affect other variables. These can be later used to constrain uncertainties when an analysis of MicroBooNE's full data set is done.

6.1.1 Neutral Pion Sideband Study

As the largest source of backgrounds MiniBooNE had, an examination of neutral pions (π^0) are necessary. In order to mimic MiniBooNE's π^0-likelihood selection, the MicroBooNE variable *pi0_score* is plotted over various ranges (where closer to 0 is more π^0-like and closer to 1 is less π^0-like). Of particular significance is the range 0.55 to 1, shown in figure 6.1, as this is the range that shows the correct reduction of π^0 events (see Chapter 5.3.4). More plots showing the effects of the NUE pre-selection and the first three selections have on the *pi0_score* variable can be found in Appendix B.

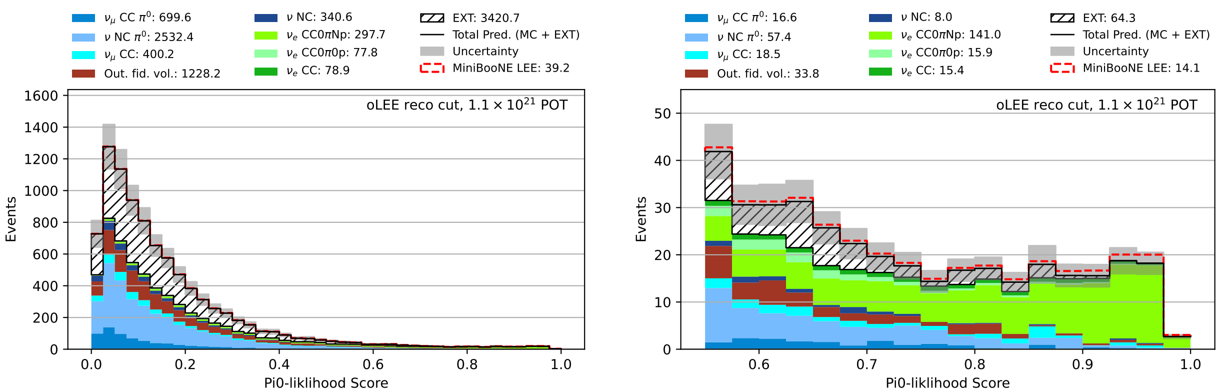

(a) The total number of π^0 is 3230.2

(b) The total number of π^0 is 74

Figure 6.1: The π^0-likelihood score plotted from 0 to 1 (left) and 0.55 to 1 (right) with the NUE pre-selection and first three selections applied. The difference in ranges represents a reduction of 97.7% π^0 events.

Using these plots, it was determined that the selection for reducing π^0 events would be set to ≥ 0.55. This reduces the background π^0 events to a level comparable to MiniBooNE. However, as noted in chapter 5.3.4, this is not exactly a MiniBooNE-like cut because it utilizes information available to the MicroBooNE detector but not the MiniBooNE detector. The discussion neeed not be repeated here; it will only be noted that a better method for replicating the MiniBooNE log-likelihood π^0 cut will be done in future studies.

6.1.2 Muon Sideband Study

Another interesting sideband is the reconstructed quasi-elastic muon neutrino energy ($E^{QE}_{\nu_\mu}$) in the same signal region as the reconstructed quasi-elastic shower neutrino energy ($E^{QE}_{\nu_e}$). This is accomplished with the same calculation as before (see equation in chapter 5.2.2), but replacing the shower energy with the muon track energy. The result can be seen in figure 6.2

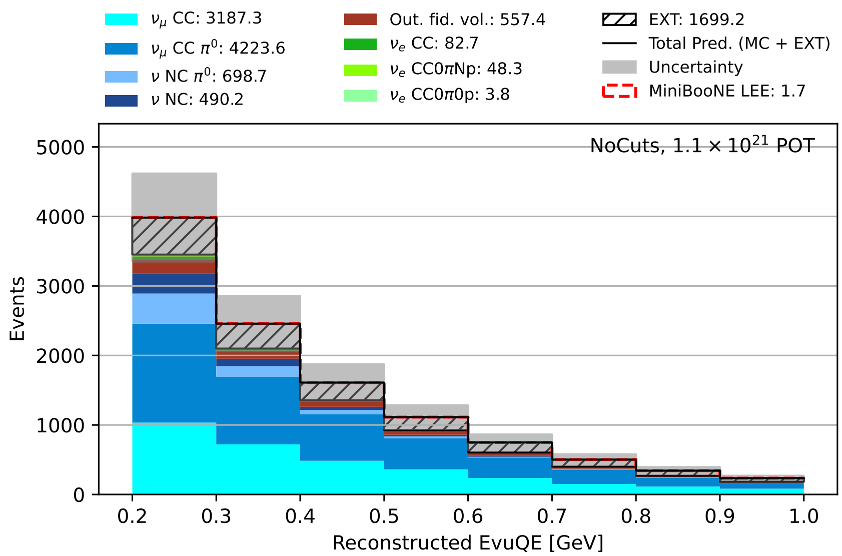

Figure 6.2: The reconstructed quasi-elastic muon neutrino energy plotted over the same range as the signal region. No pre-selection or cuts have been applied.

More plots of the reconstructed quasi-elastic muon neutrino energy can be seen in Appendix B.

6.1.3 High Energy Range (1-3 GeV) Sideband Study

The final sideband is an examination of the reconstructed quasi-elastic shower neutrino energy in the high energy range (1-3 GeV) fully outside the signal region. Here it can be clearly seen how the pre-selection and each selection affect the variable without looking at the signal region. This will be important for both open data comparisons and later unblinding the full analysis.

Full selection by selection plots can be seen in Appendix B in figures B.7 through B.9. Here in figure 6.3 we examine the overall affect from both the pre-selection and all four selections applied. It can clearly be seen that while a large reduction in the out-of-fiducial-volume and EXT events occurs, a large reduction in π^0 events occurs as well. This demonstrates what appears to be a MiniBooNE-like reduction in these background events. However, to better resemble MiniBooNE's log-likelihood π^0 selection the method stated in 5.3.4 should be used.

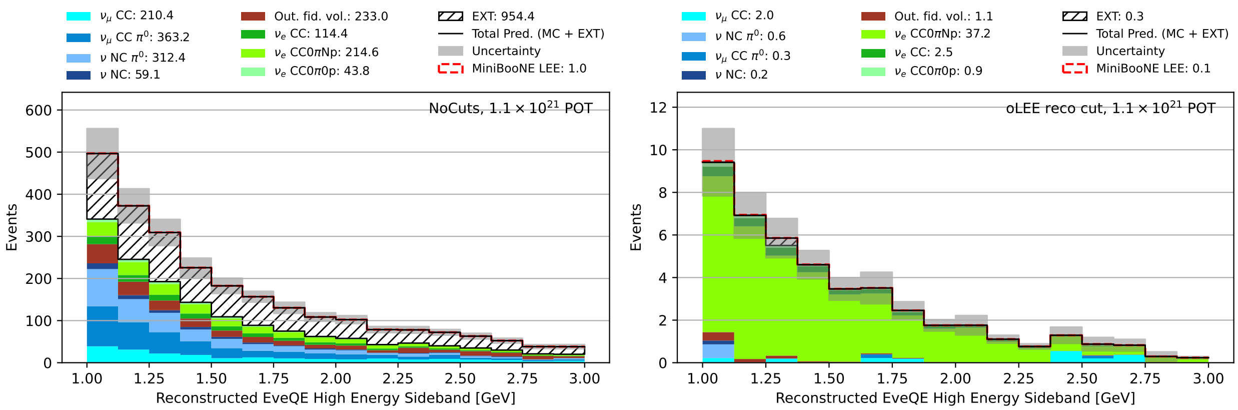

(a) No pre-selection or selections applied.

(b) All 4 selections applied.

Figure 6.3: The reconstructed quasi-elastic shower neutrino energy plotted over the high energy range (1-3 GeV) with and without the NUE pre-selection and all selections applied.

6.2 Open Data Comparison

MicroBooNE has a small subset of data available for analysis purposes without going through the full unblinding procedures. This small subset is used here to look at the signal region of the reconstructed quasi-elastic energy. Unfortunately, but unsurprisingly, given the selected signal and the already low number of events no statistical claims can be made here about the open data plots. One can be seen here in figure 6.4, the reconstructed quasi-elastic neutrino energy. The reader will note the even lower number of events compared to the full Monte Carlo plots, as well as the fact that some bins have no data at all. The rest can be seen in Appendix C. The reader can view a discussion of the sensitivity of this study and final conclusions in Chapter 7.

6.3 Uncertainties

The uncertainty calculations involved in both the Monte Carlo only and open data plots are discussed here, including the detector systematics and the built-in uncertainties used in the PeLEE modeling. The PeLEE framework has several sources of uncertainty including the model of the BNB flux, the models of neutrino interactions, and the model of the MicroBooNE detector behavior.

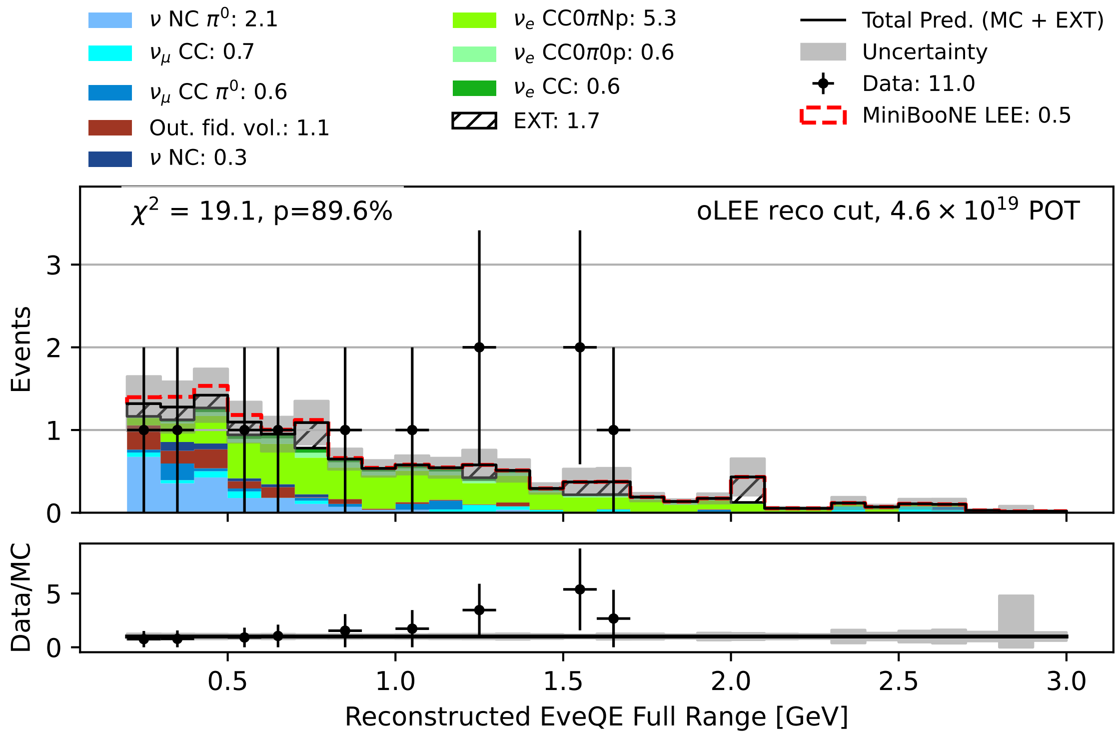

Figure 6.4: The reconstructed quasi-elastic neutrino energy over the full range (signal plus the high energy sideband). Note the even lower number of events, and that some bins have no data at all.

Hadron production cross sections are one of the primary sources of uncertainty in the model of the BNB flux, particularly $\pi^{\pm}$, $K^{\pm}$, and K^0_L produced in the BNB. The other primary source of uncertainty comes from the design and current of the BNB horn, and the secondary interactions from the aluminum horn and the beryllium target. The PeLEE framework treats these uncertainties similarly to other cross section analyses done by the MicroBooNE collaboration.[4]

As mentioned in Chapter 5.1, the PeLEE framework utilizes GENIE v3.0.6 G18_10a_02_11a to model detector neutrino interactions and the final state particles those interactions produce. This was accomplished differently depending on the particular parameter. Some parameters were estimated using a specialized tune of the GENIE model, and the uncertainties were extracted from those fits. Other parameter uncertainties not estimated by the tune were given by the GENIE Collaboration. Any parameters where the GENIE Collaboration did not provide unertainties for were estimated by he PeLEE group in various ways as noted in their paper.[4]

The MicroBooNE Collaboration models different detector systems through a variety of means that the PeLEE framework relies to account for detector uncertainties, of which further details can be found in the cited papers.[3;4] While most of the uncertainty calculations built into the PeLEE framework are done automatically, detector systematics and uncertainties must be added in separately. Therefore, detector systemics and the relevant uncertainties have not yet been added to the uncertainty calculations in this study, and will need to be in the future to ensure a full accounting for all uncertainties is completed. In figure 6.5, the correlation matrix for the full range of the reconstructed quasi-elastic neutrino energy for both the Monte Carlo and open data can be seen. The interested reader may view the other correlation matrices that aid in the uncertainty calculations in Appendix C.

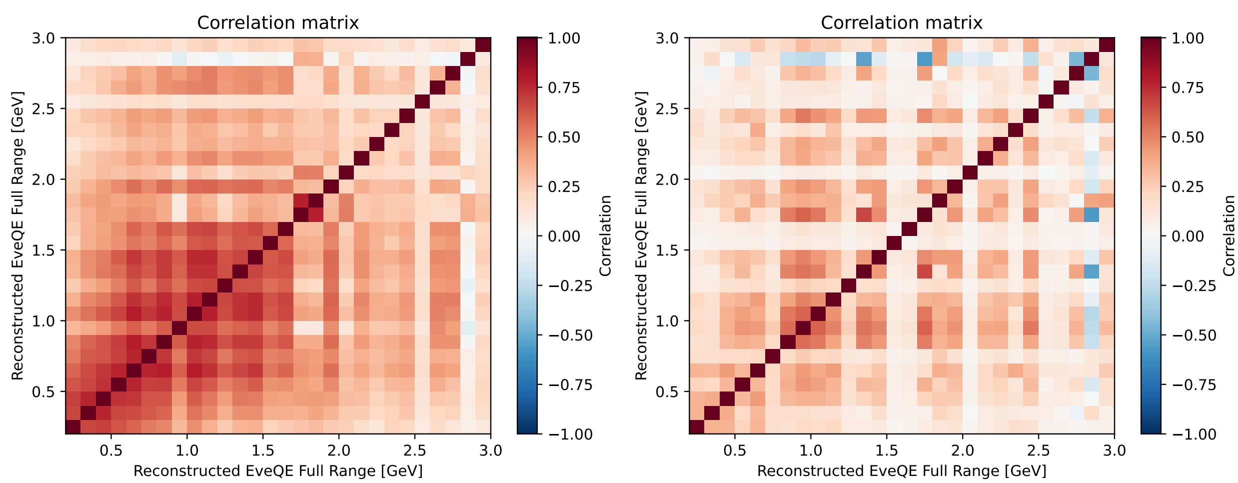

(a) Monte Carlo (b) Open Data

Figure 6.5: The correlation matrices for the full range (0.2-3 GeV) of the reconstructed quasi-elastic neutrino energy.

Chapter 7

Conclusions

This chapter discusses the sensitivity of this study, draws some final conclusions, and ends with suggested next steps for this study.

7.1 Sensitivity of this Analysis and Conclusions

A sensitivity calculation is necessary to answer the fundamental question of this study: is the MicroBooNE experiment sensitive enough to the selected signal to allow for a full analysis? as can be seen in figure 7.1, the binning has been altered to look for an excess located in the first bin (0.2 to 0.9 GeV).

The χ^2 is calculated for the first bin where the excess could be found:

$$\chi^2 = \sum_{i=1} \frac{(N_i - \mu_i)^2}{\sigma^2_{N_i+\mu_i}}$$

$$\chi^2 = \frac{(N_1 - \mu_1)^2}{\sigma^2_{N_1+\mu_1}}$$

$$\chi^2 = \frac{(N_1 - \mu_1)^2}{N_1 + \sigma^2_{\mu_1}}$$

where N_1 is the Monte Carlo prediction (black line) plus some number times the modeled LEE prediction (red dashed line) of the first bin, μ_1 is the Monte Carlo prediction of the

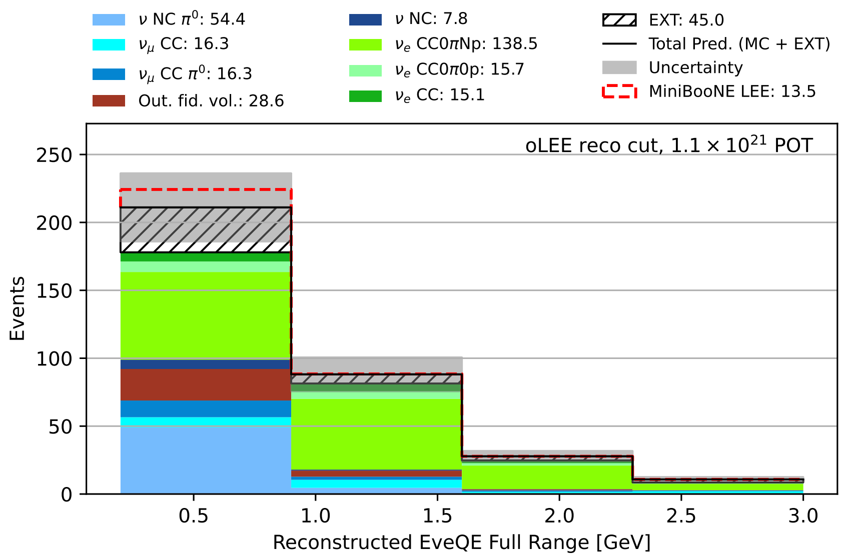

Figure 7.1: The reconstructed quasi-elastic muon neutrino energy plotted over the full range (0.2-3 GeV) and re-binned so that an excess would be located only in the first bin and not affect any higher energy bins.

first bin, and σ_{μ_1} is the uncertainty of the first bin. Plugging that into the prior equation yields

$$\chi^2 = \frac{(Pred_{MC} + x \cdot Pred_{LEE} - Pred_{MC})^2}{Pred_{MC} + x \cdot Pred_{LEE} + \sigma_{\mu_1}^2}$$

$$\chi^2 = \frac{x^2 \cdot Pred_{LEE}^2}{Pred_{MC} + x \cdot Pred_{LEE} + \sigma_{\mu_1}^2}$$

Plugging in numbers extracted from figure 7.1 gives

$$\chi^2 = \frac{x^2 \cdot (12.6)^2}{211.1 + x \cdot (12.6) + (24.7)^2}$$

which now gives a simple algebraic problem of determining x for a given χ^2 value. For two standard deviations, one degree of freedom, and a p-value of 0.05, a χ^2 value of four is desired. Plugging that in and completing the problem yields a sensitivity of

$$x \approx 4.7$$

In order to see a 2σ excess somewhere in the signal region (0.2 - 0.9 GeV), the number of events would need to be 4.7 times the modeled MiniBooNE LEE.

7.2 Next Steps

Before comparing to the full MicroBooNE data set, several things can be done to further improve this study. As mentioned in Chapter 5.3.4, the neutral pion selection should be improved to more closely match MiniBooNE's version of this selection. Rather than using the *pi0_score* variable, which contains information from the MicroBooNE detector that the MiniBooNE detector would not have had, an equation that is dependent on the visible energy should be developed and fit to the Monte Carlo in order to determine a similar selection to MiniBooNE.[26]

As also mentioned in Chapter 6, the sidebands developed in this study can be used to further constrain the uncertainty in the signal region and reduce the sensitivity necessary to see a MiniBooNE-like excess in MicroBooNE's data. This can be done by examining and establishing what the reduced uncertainties are in the various sidebands (neutral pion, muon, and high energy). The purpose of the sidebands is to look in a region and at a variable that would not be affected by an changes that occur in the signal region. Those reduced uncertainties from the sidebands can then be applied to the signal region to further reduce uncertainties in the signal region.

Bibliography

[1] A. A. Aguilar-Arevalo et al. Significant Excess of ElectronLike Events in the MiniBooNE Short-Baseline Neutrino Experiment. *Phys. Rev. Lett.*, 121(22):221801, 2018. doi: 10.1103/PhysRevLett.121.221801. URL https://journals.aps.org/prl/abstract/10.1103/PhysRevLett.121.221801.

[2] Alan Chodos et al. *Ghost Particle: In Search of the Elusive and Mysterious Neutrino*. The MIT Press, 1st edition, 2023.

[3] R. Acciarri et al. Design and construction of the microboone detector. *JINST*, 12(02):P02017, 2017. doi: 10.1088/1748-0221/12/02/P02017. URL https://www.osti.gov/pages/biblio/1346368.

[4] P. Abratenko et al. Search for an anomalous excess of charged-current ν_e interactions without pions in the final state with the microboone experiment. *Phys. Rev. D*, 105:112004, Jun 2022. doi: 10.1103/PhysRevD.105.112004. URL https://link.aps.org/doi/10.1103/PhysRevD.105.112004.

[5] P. Abratenko et al. Search for neutrino-induced neutral-current Δ radiative decay in microboone and a first test of the miniboone low energy excess under a single-photon hypothesis. *Phys. Rev. Lett.*, 128:111801, Mar 2022. doi: 10.1103/PhysRevLett.128.111801. URL https://link.aps.org/doi/10.1103/PhysRevLett.128.111801.

[6] P. Abratenko et al. Search for an anomalous excess of charged-current quasielastic ν_e interactions with the microboone experiment using deep-learning-based reconstruction. *Phys. Rev. D*, 105:112003, Jun 2022. doi: 10.1103/PhysRevD.105.112003. URL https://link.aps.org/doi/10.1103/PhysRevD.105.112003.

[7] P. Abratenko et al. Search for an anomalous excess of inclusive charged-current ν_e interactions in the microboone experiment using wire-cell reconstruction. *Phys. Rev. D*, 105:112005, Jun 2022. doi: 10.1103/PhysRevD.105.112005. URL https://link.aps.org/doi/10.1103/PhysRevD.105.112005.

[8] P. Abratenko et al. Search for an excess of electron neutrino interactions in microboone using multiple final-state topologies. *Phys. Rev. Lett.*, 128:241801, Jun 2022. doi: 10.1103/PhysRevLett.128.241801. URL https://link.aps.org/doi/10.1103/PhysRevLett.128.241801.

[9] The MicroBooNE Collaboration. Inclusive search for anomalous single-photon production in microboone, 2025. URL https://arxiv.org/abs/2502.06064.

[10] E. H. Yandel. *A Search for Anomalous Single Photon Production in Neutrino Interactions with the MicroBooNE Detector*. PhD thesis, UC Santa Barbara, 2024. URL https://escholarship.org/uc/item/6rq082dr.

[11] A. A. Aguilar-Arevalo et al. The MiniBooNE Detector. *Nucl. Instrum. Meth. A*, 599:28–46, 2009. doi: 10.1016/j.nima.2008.10.028. URL https://inspirehep.net/literature/789156.

[12] A. A. Aguilar-Arevalo et al. Updated miniboone neutrino oscillation results with increased data and new background studies. *Phys. Rev. D*, 103:052002, Mar 2021. doi: 10.1103/PhysRevD.103.052002. URL https://link.aps.org/doi/10.1103/PhysRevD.103.052002.

[13] Michael F. L'Annunziata. *Radioactivity: Introduction and History*. Elsevier Science & Technology, 2007.

[14] Alessandro Bettini. *Introduction to Elementary Particle Physics*. Cambridge University Press, 3rd edition, 2024.

[15] C. Adams et al. Ionization electron signal processing in single phase lartpcs. part i. algorithm description and quantitative evaluation with microboone simulation. *JINST*,

13(07):P07006, Jul 2018. doi: 10.1088/1748-0221/13/07/P07006. URL https://doi.org/10.1088/1748-0221/13/07/P07006.

[16] P. Adamson et al. The numi neutrino beam. *Nucl. Instrum. Meth. A*, 806:279–306, Jan 2016. ISSN 0168-9002. doi: 10.1016/j.nima.2015.08.063. URL http://dx.doi.org/10.1016/j.nima.2015.08.063.

[17] R. Acciarri et al. The pandora multi-algorithm approach to automated pattern recognition of cosmic-ray muon and neutrino events in the microboone detector. *Eur. Phys. J. C*, 78(82), Jan 2018. doi: 10.1140/epjc/s10052-017-5481-6. URL https://doi.org/10.1140/epjc/s10052-017-5481-6.

[18] P. Abratenko et al. First constraints on light sterile neutrino oscillations from combined appearance and disappearance searches with the microboone detector. *Phys. Rev. Lett.*, 130:011801, Jan 2023. doi: 10.1103/PhysRevLett.130.011801. URL https://link.aps.org/doi/10.1103/PhysRevLett.130.011801.

[19] P. Abratenko et al. Search for an anomalous production of charged-current ν_e interactions without visible pions across multiple kinematic observables in microboone. *Physical Review Letters*, 135(8), aug 2025. ISSN 1079-7114. doi: 10.1103/x259-z6mf. URL http://dx.doi.org/10.1103/x259-z6mf.

[20] P. Abratenko et al. Enhanced search for neutral current Δ radiative single-photon production in microboone. *Physical Review D*, 112(9), nov 2025. ISSN 2470-0029. doi: 10.1103/49ds-5hfh. URL http://dx.doi.org/10.1103/49ds-5hfh.

[21] R. Brun and F. Rademakers. ROOT: An object oriented data analysis framework. *Nucl. Instrum. Meth. A*, 389:81–86, 1997. doi: 10.1016/S0168-9002(97)00048-X. URL https://ui.adsabs.harvard.edu/abs/1997NIMPA.389...81B/abstract.

[22] R.B. Patterson, E.M. Laird, Y. Liu, P.D. Meyers, I. Stancu, and H.A. Tanaka. The extended-track event reconstruction for miniboone. *Nuclear Instruments and Methods in Physics Research Section A: Accelerators, Spectrometers, Detectors and Associated*

Equipment, 608(1):206–224, Sep 2009. ISSN 0168-9002. doi: 10.1016/j.nima.2009.06.064. URL http://dx.doi.org/10.1016/j.nima.2009.06.064.

[23] P. Abratenko et al. New CC0π genie model tune for microboone. *Phys. Rev. D*, 105: 072001, Apr 2022. doi: 10.1103/PhysRevD.105.072001. URL https://link.aps.org/doi/10.1103/PhysRevD.105.072001.

[24] J. Allison et al. Recent developments in geant4. *Nuclear Instruments and Methods in Physics Research Section A: Accelerators, Spectrometers, Detectors and Associated Equipment*, 835:186–225, 2016. ISSN 0168-9002. doi: https://doi.org/10.1016/j.nima.2016.06.125. URL https://www.sciencedirect.com/science/article/pii/S0168900216306957. https://geant4.web.cern.ch/.

[25] Eric D. Church. Larsoft: A software package for liquid argon time projection drift chambers, 2014. URL https://arxiv.org/abs/1311.6774. https://larsoft.org/.

[26] Kevin J. Kelly and Joachim Kopp. More ingredients for an altarelli cocktail at miniboone. *Journal of High Energy Physics*, 2023(5), may 2023. ISSN 1029-8479. doi: 10.1007/jhep05(2023)113. URL http://dx.doi.org/10.1007/JHEP05(2023)113.

Appendix A

Full Selection Plots

This appendix contains all the variable plots studied before and after cuts were implemented. First is number of Cherenkov-visible showers before and after colinear recombination in figures A.1 through A.6. The plots show a statistical insignificance in the event count, however the recombination variable was used for completeness purposes and to better mimic MiniBooNE's analysis. Following that will be the shower score and shower theta plots in figures A.7 through A.12.

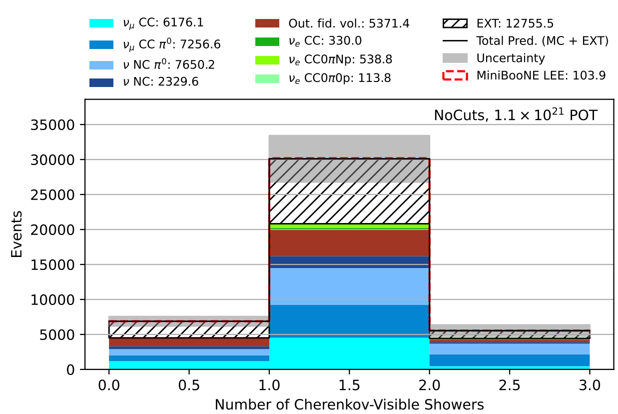

(a) nshr_visible variable.

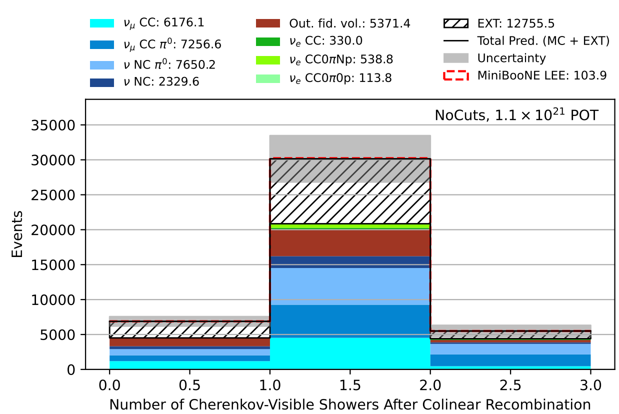

(b) nshr_mB_vis variable.

Figure A.1: Cherenkov-visible shower variables without the NUE pre-selection or selections applied.

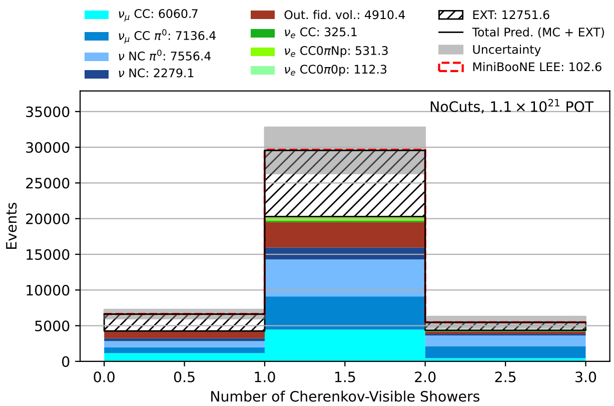

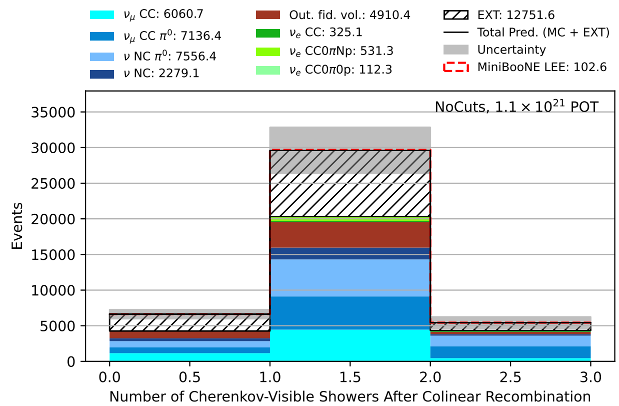

(a) nshr_visible variable.

(b) nshr_mB_vis variable.

Figure A.2: Cherenkov-visible shower variables with only the NUE pre-selection applied.

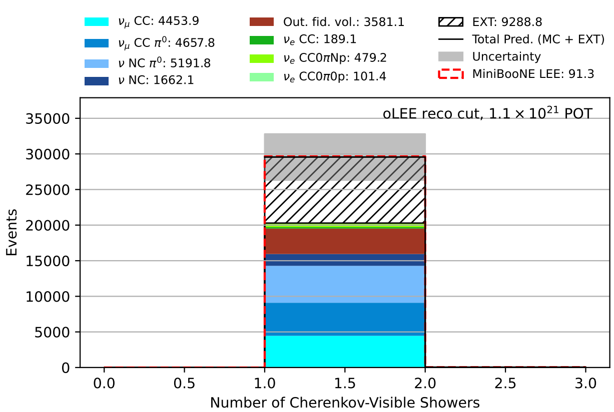

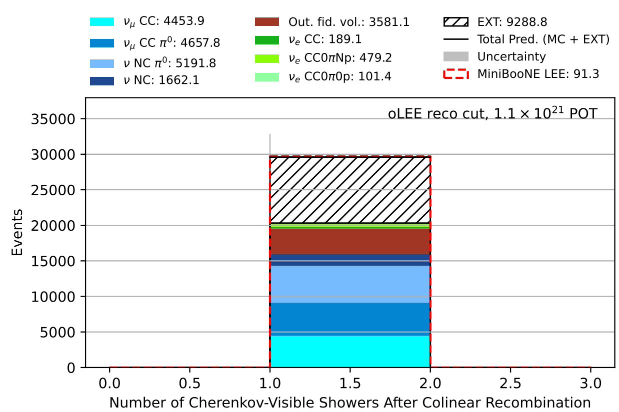

(a) nshr_visible variable.

(b) nshr_mB_vis variable.

Figure A.3: Cherenkov-visible shower variables with the NUE pre-selection and selection 1 applied.

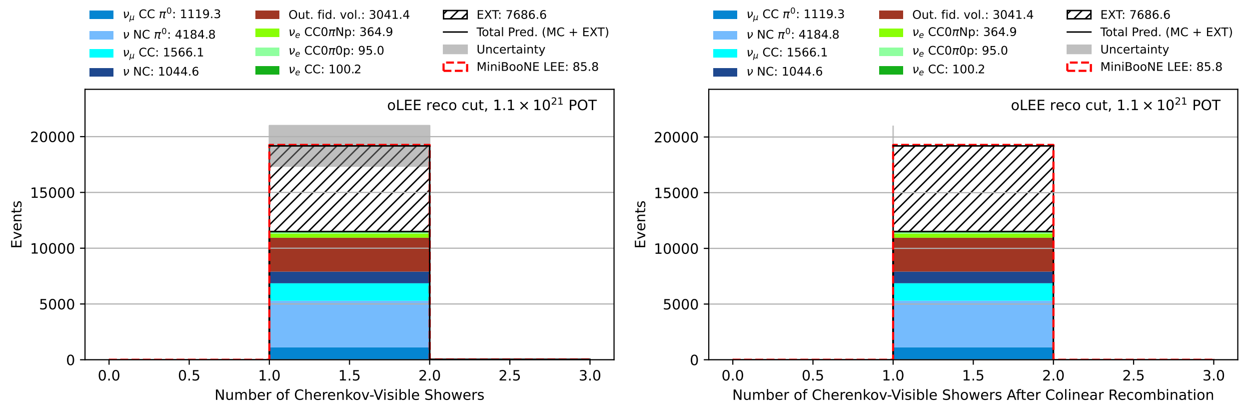

(a) nshr_visible variable. (b) nshr_mB_vis variable.

Figure A.4: Cherenkov-visible shower variables with the NUE pre-selection and selections 1 and 2 applied.

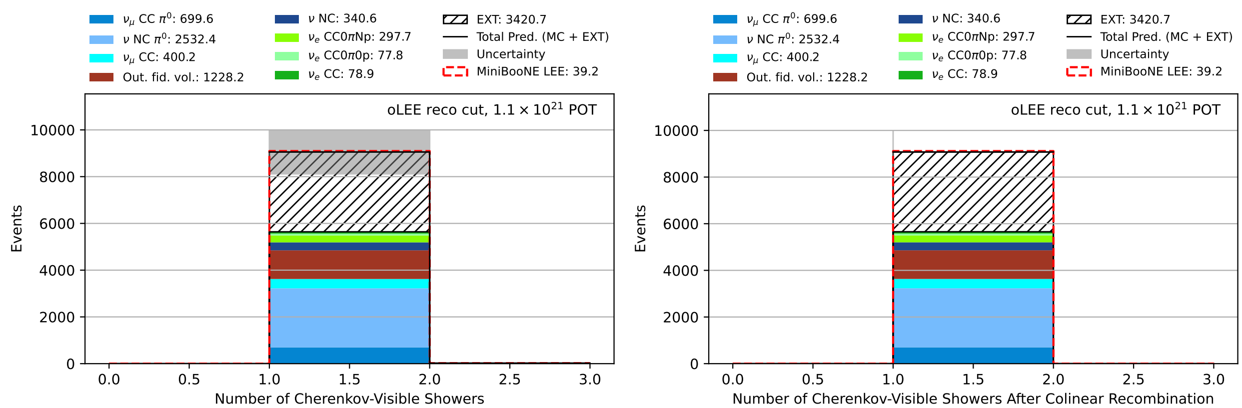

(a) nshr_visible variable. (b) nshr_mB_vis variable.

Figure A.5: Cherenkov-visible shower variables with the NUE pre-selection and selections 1, 2, and 3 applied.

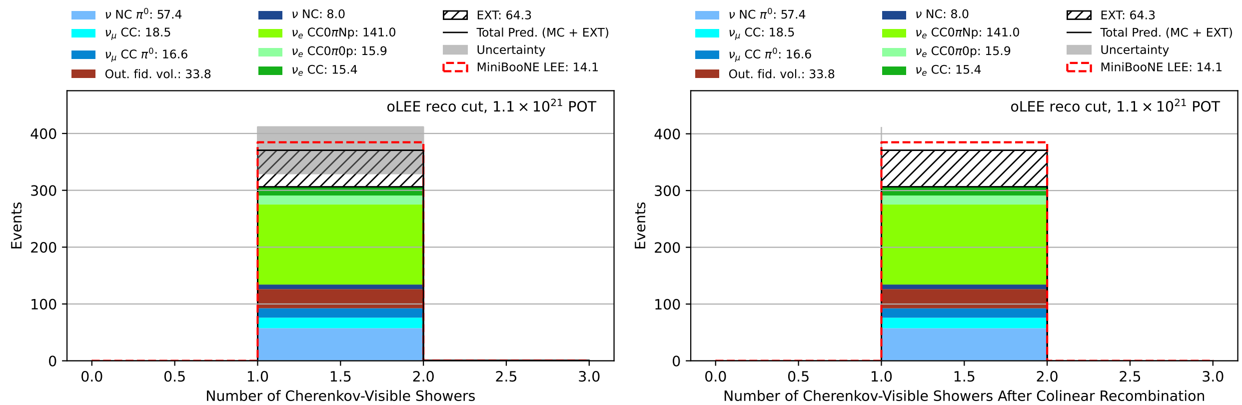

(a) nshr_visible variable.

(b) nshr_mB_vis variable.

Figure A.6: Cherenkov-visible shower variables with the NUE pre-selection and all 4 selections applied.

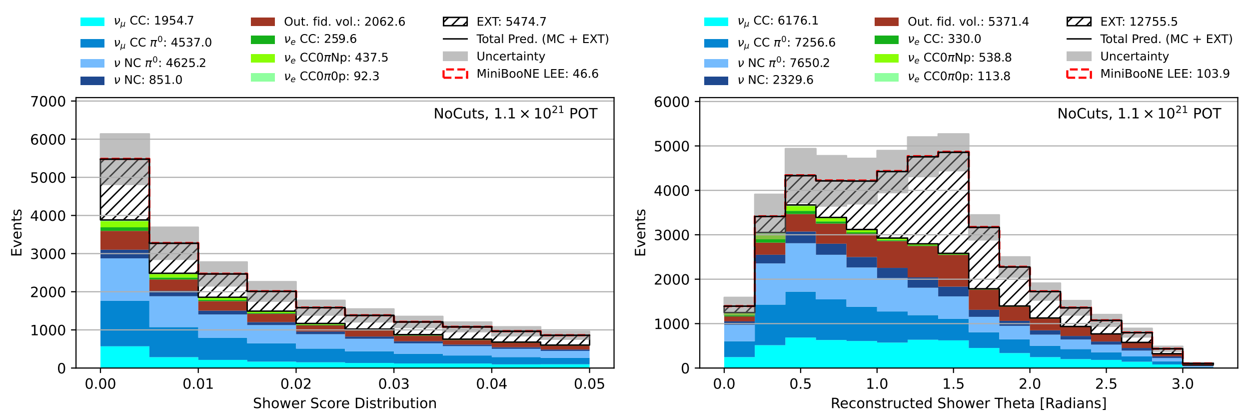

(a) shr_score variable.

(b) shr_theta variable.

Figure A.7: Shower score and shower θ variables without the NUE pre-selection or selections applied.

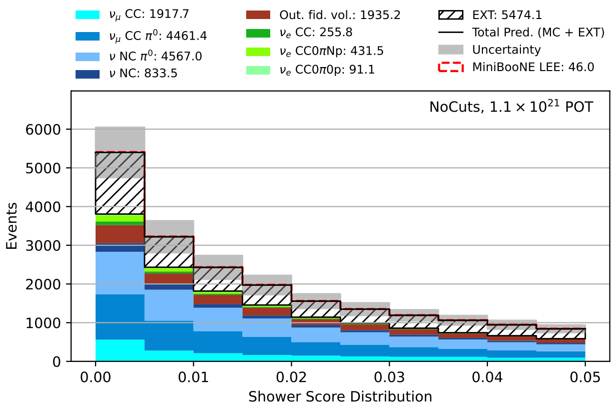

(a) shr_score variable.

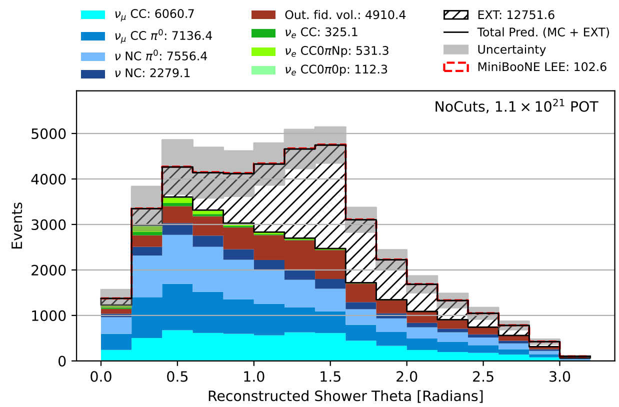

(b) shr_theta variable.

Figure A.8: Shower score and shower θ variables with only the NUE pre-selection applied.

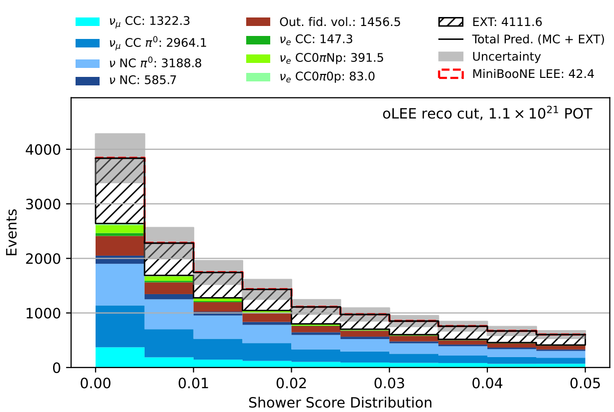

(a) shr_score variable.

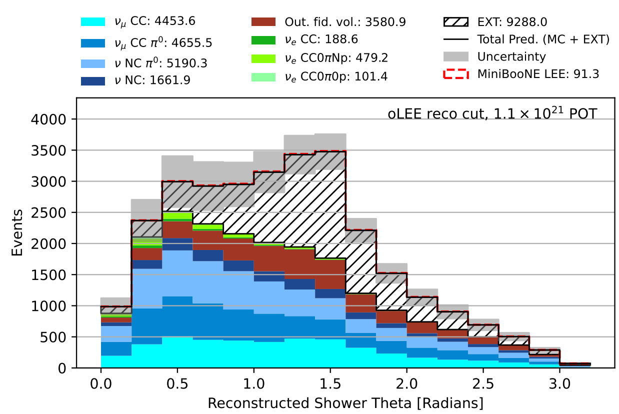

(b) shr_theta variable.

Figure A.9: Shower score and shower θ variables with the NUE pre-selection and selection 1 applied.

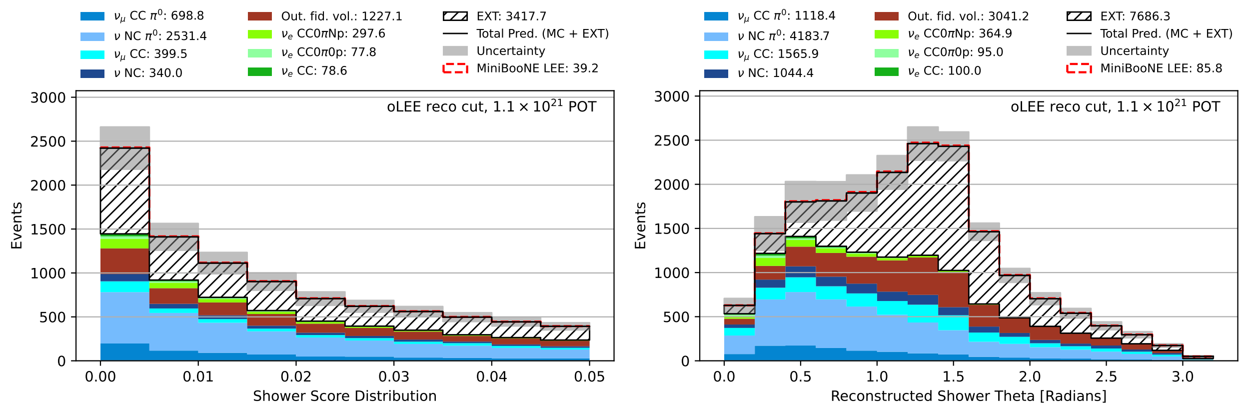

(a) shr_score variable.

(b) shr_theta variable.

Figure A.10: Shower score and shower θ variables with the NUE pre-selection and selections 1 and 2 applied.

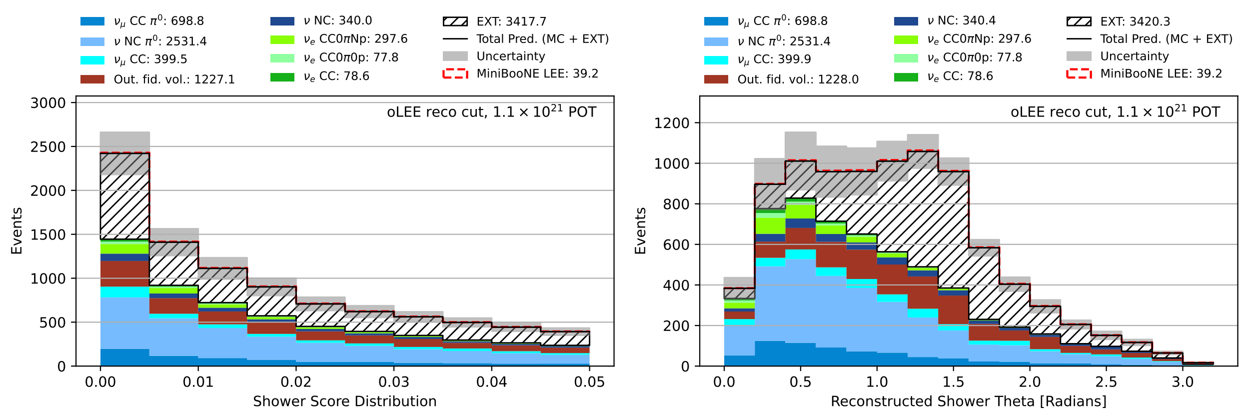

(a) shr_score variable.

(b) shr_theta variable.

Figure A.11: Shower score and shower θ variables with the NUE pre-selection and selections 1, 2, and 3 applied.

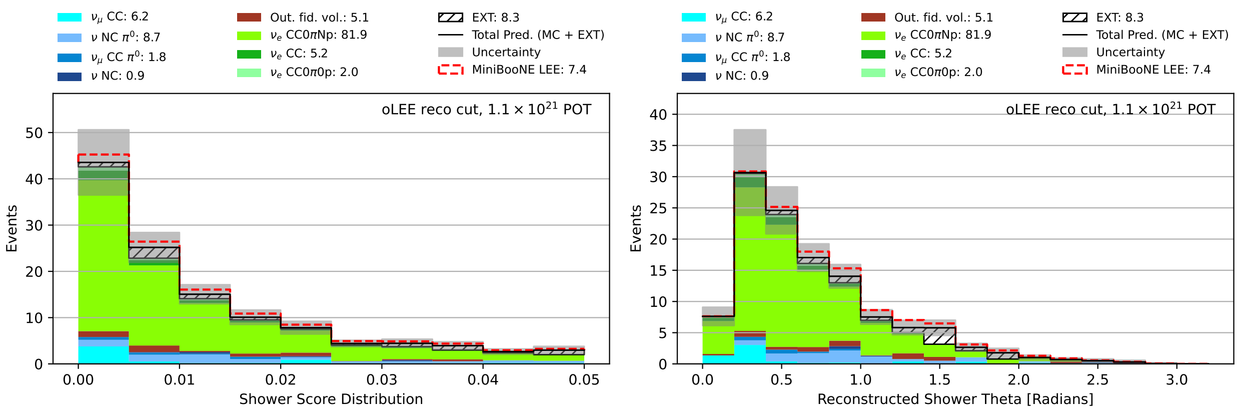

(a) shr_score variable.

(b) shr_theta variable.

Figure A.12: Shower score and shower θ variables with the NUE pre-selection and all 4 selections applied.

Appendix B

Full Sideband Plots

This appendix contains all the sideband plots. First are the neutral pion sideband plots in figures B.1 through B.4. The plots show the steps to determining the *pi0_score* selection. Following that will be the reconstructed quasi-elastic muon neutrino plots in figures B.5 and B.6 . Finally, the high energy sideband plots will be in figures B.7 through B.12. These include not only the reconstructed quasi-elastic neutrino energy, but also the other variables seen in Appendix A plotted only for events in the high energy range (1-3 GeV).

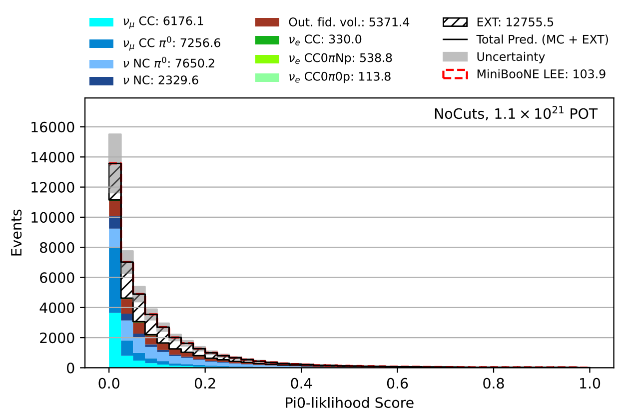

(a) No pre-selection or selections applied.

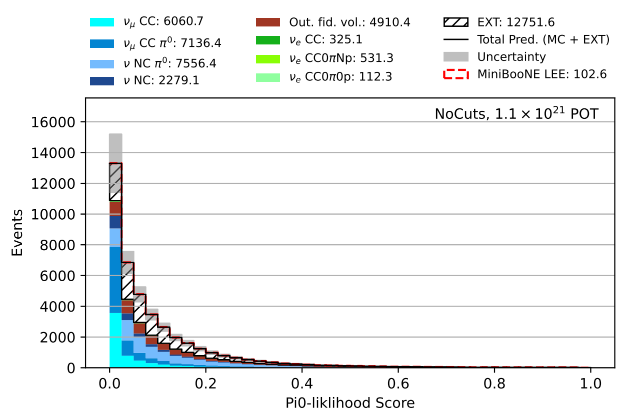

(b) Only the NUE pre-selection applied.

Figure B.1: pi0_score variable with no pre-selection or selections (left) and only the NUE pre-selection (right) applied.

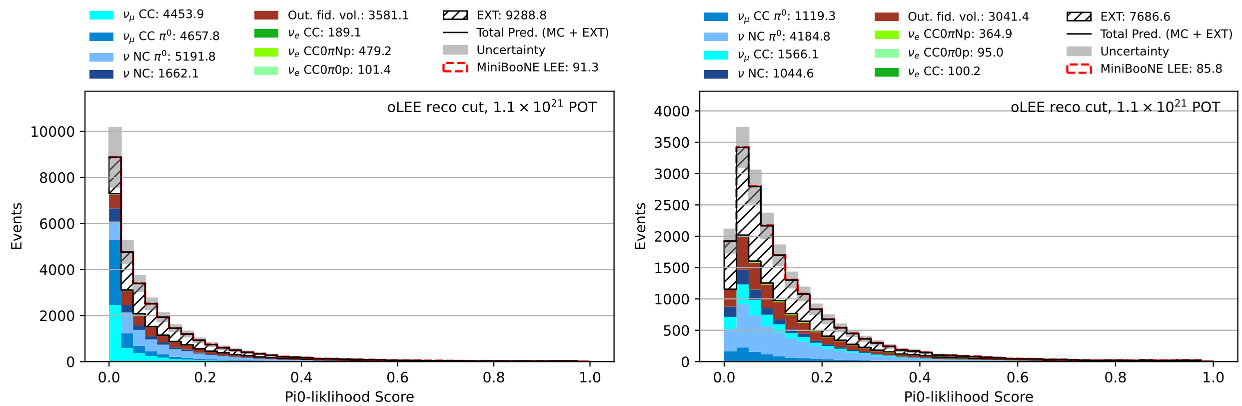

(a) Selection 1 applied.

(b) Selections 1 and 2 applied.

Figure B.2: pi0_score variable with the NUE pre-selection and selection 1 (left) and 2 (right) applied.

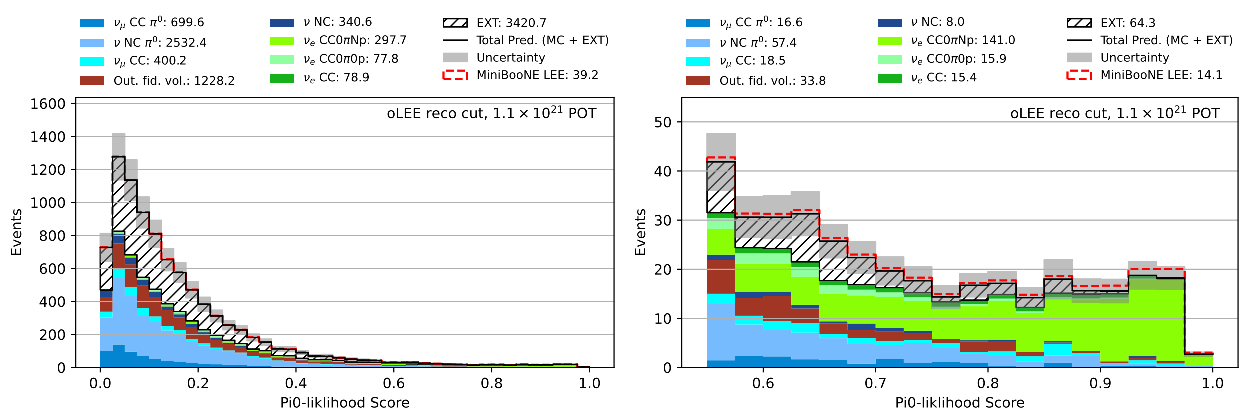

(a) Full range.

(b) Range of 0.55 - 1 for final selection.

Figure B.3: pi0_score variable with the NUE pre-selection and selections 1, 2, and 3 applied. The right plot represents the range where the correct event reduction takes place, and was the final selected value for the neutral pion selection (selection 4).

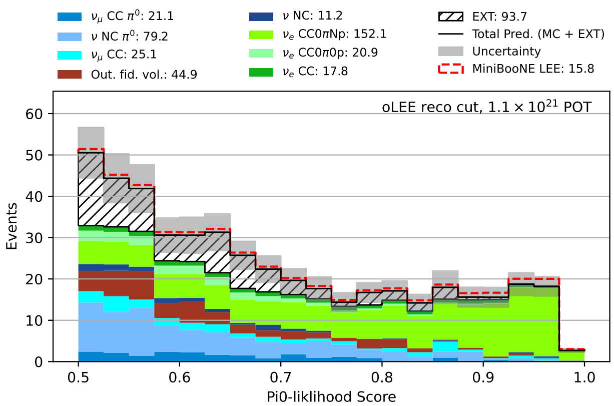

(a) Range of 0.5 - 1

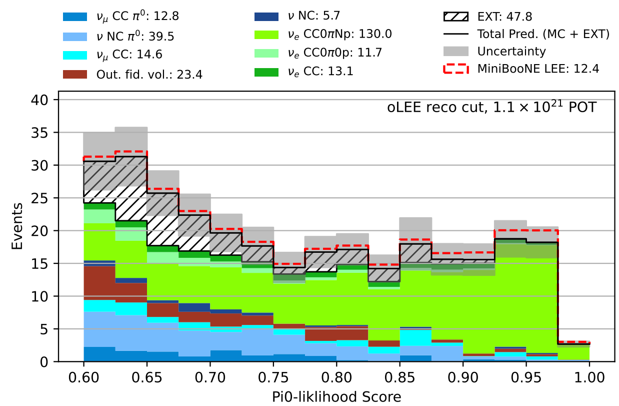

(b) Range of 0.6 - 1

Figure B.4: pi0_score variable with the NUE pre-selection and selections 1, 2, and 3 applied. These were the first two ranges checked to determine if the correct event reduction had taken place.

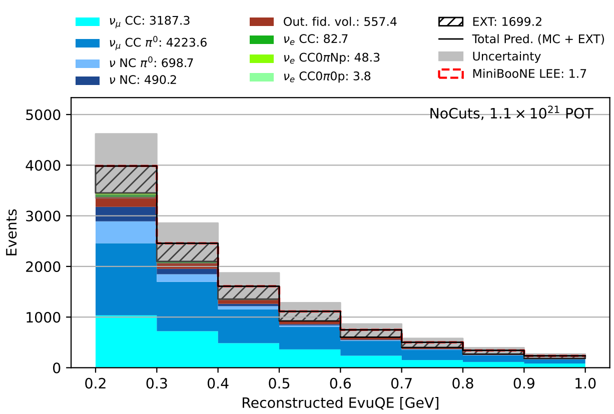

(a) No pre-selection or selections applied.

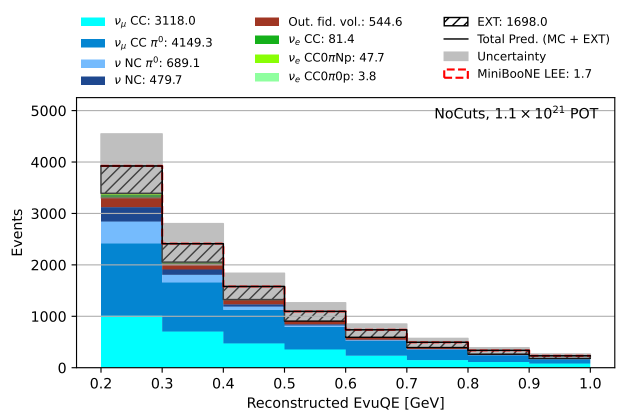

(b) Only the NUE pre-selection applied.

Figure B.5: The reconstructed quasi-elastic muon neutrino energy plotted over the same range as the signal region with and without the NUE pre-selection applied.

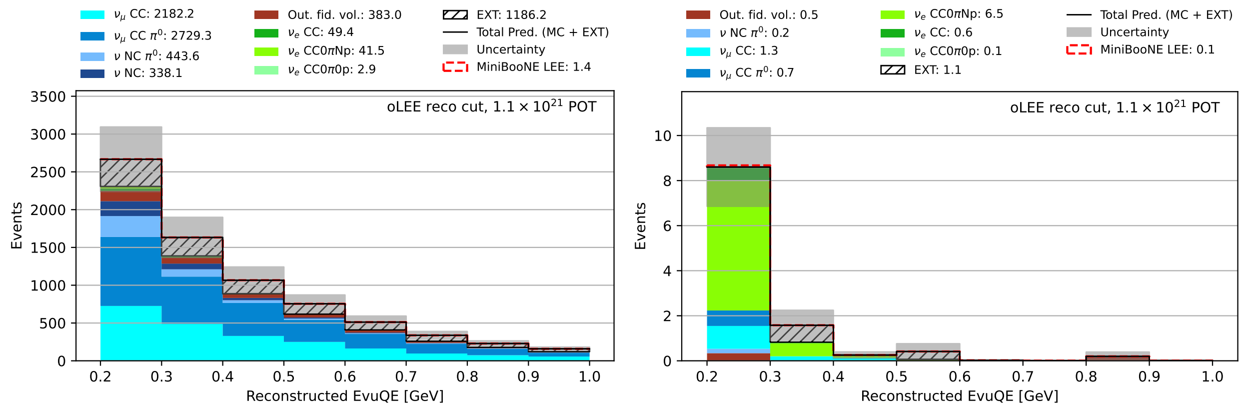

(a) Selection 1 applied. (b) Selections 1 and 4 applied.

Figure B.6: The reconstructed quasi-elastic muon neutrino energy plotted over the same range as the signal region with the NUE pre-selection and other selections applied.

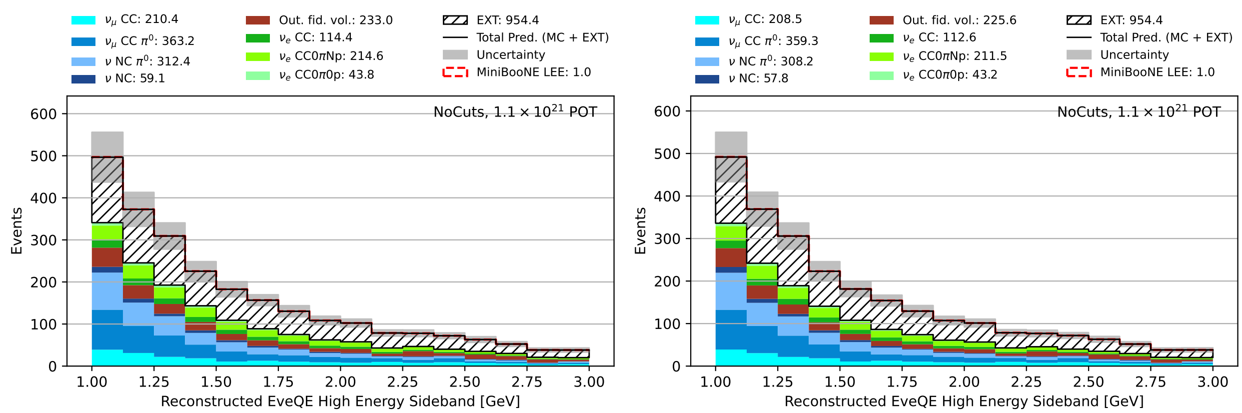

(a) No pre-selection or selections applied. (b) Only the NUE pre-selection applied.

Figure B.7: The reconstructed quasi-elastic shower neutrino energy plotted over the high energy range (1-3 GeV) with and without the NUE pre-selection applied.

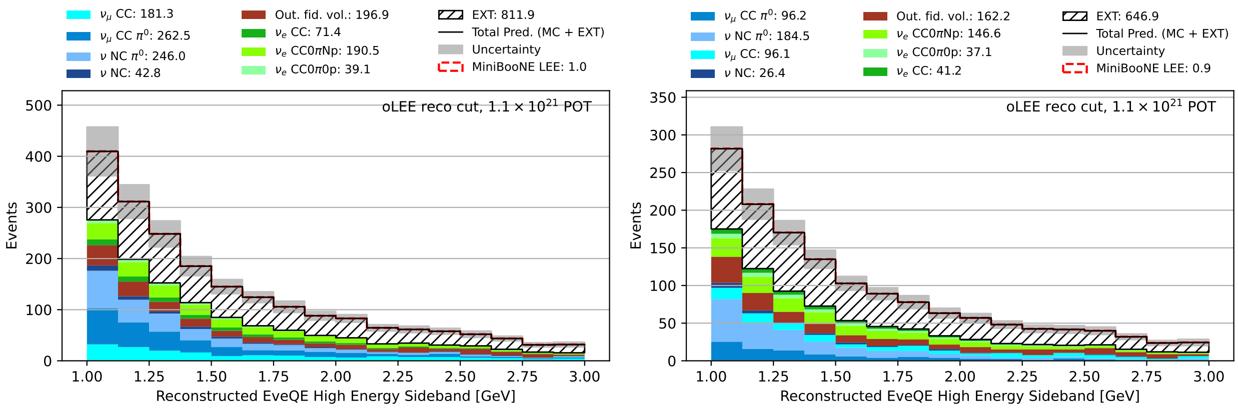

(a) Selection 1 applied.

(b) Selections 1 and 2 applied.

Figure B.8: The reconstructed quasi-elastic shower neutrino energy plotted over the high energy range (1-3 GeV) with the NUE pre-selection and other selections applied.

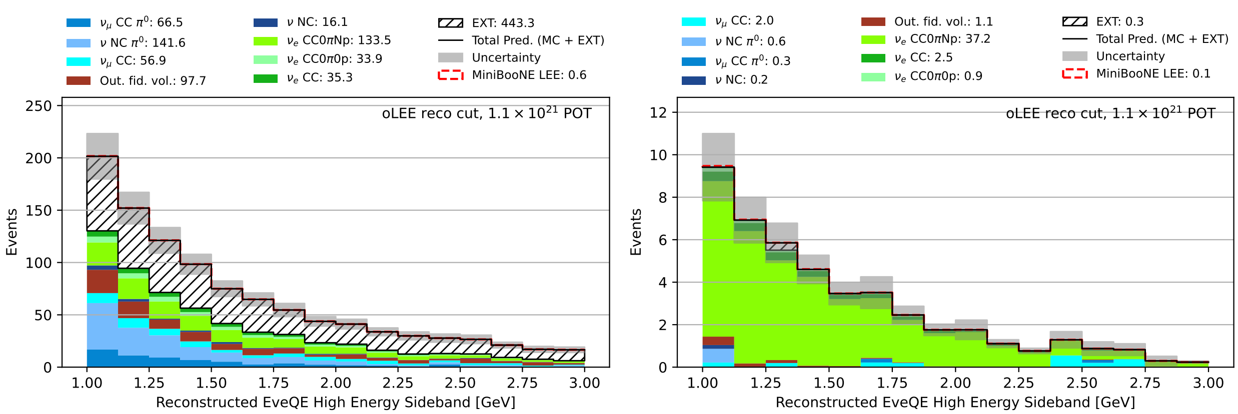

(a) Selection 1, 2, and 3 applied.

(b) All 4 selections applied.

Figure B.9: The reconstructed quasi-elastic shower neutrino energy plotted over the high energy range (1-3 GeV) with the NUE pre-selection and other selections applied.

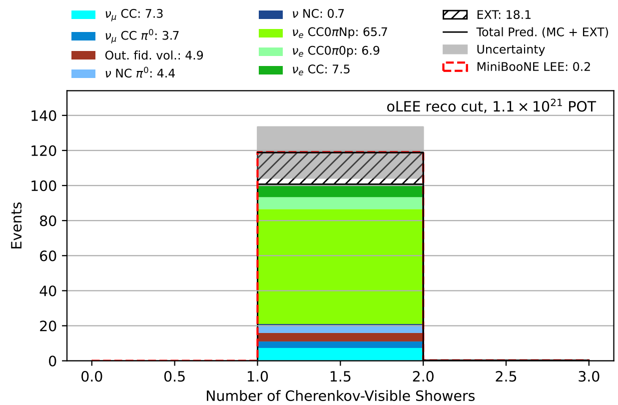

(a) nshr_visible variable

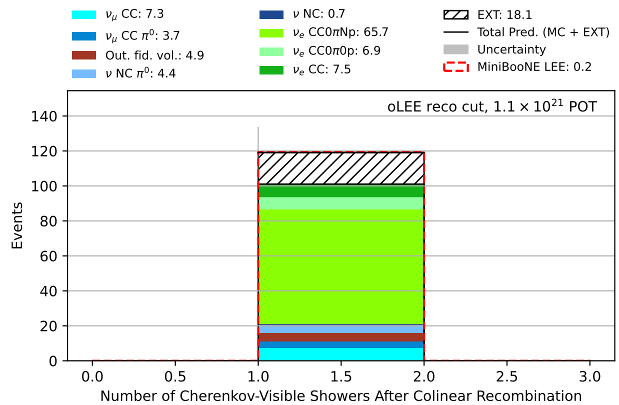

(b) nshr_mB_vis variable

Figure B.10: The nshr_visible (left) and nshr_mB_vis variables plotted for events in the high energy range (1-3 GeV) with the NUE pre-selection and all 4 selections applied.

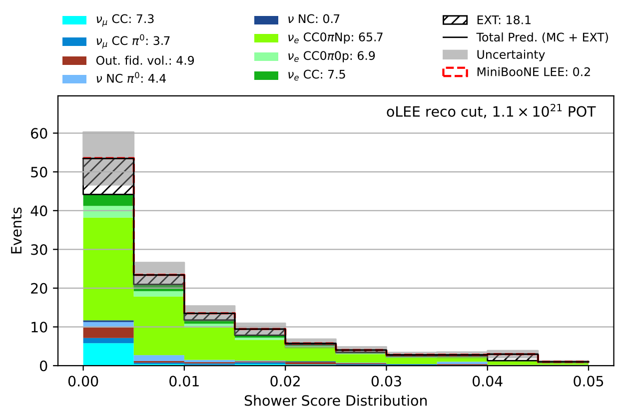

(a) nshr_visible variable

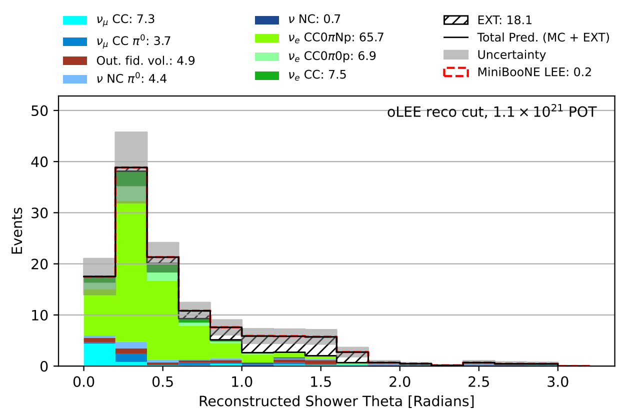

(b) nshr_mB_vis variable

Figure B.11: The shr_score (left) and shr_theta variables plotted for events in the high energy range (1-3 GeV) with the NUE pre-selection and all 4 selections applied.

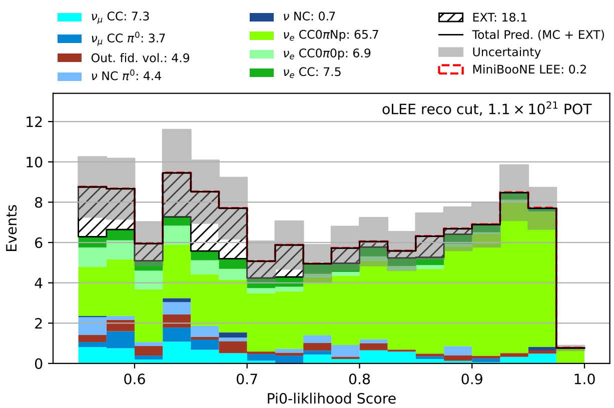

(a) pi0_score variable

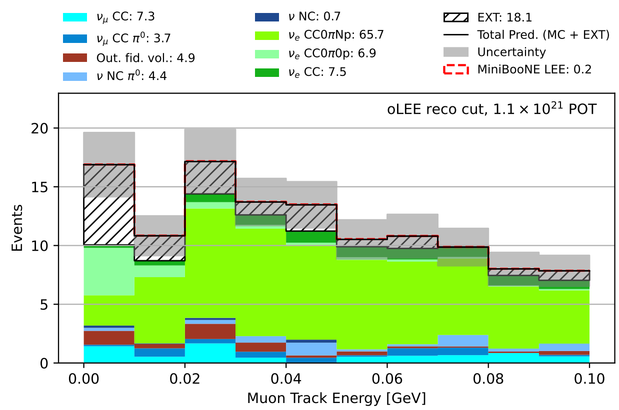

(b) trk_energy_muon variable

Figure B.12: The pi0_score (left) and trk_energy_muon variables plotted for events in the high energy range (1-3 GeV) with the NUE pre-selection and all 4 selections applied.

Appendix C

Open Data Plots and Correlation Matrices

In this appendix,the reader will find all of the open data plots, as well as the correlation matrices for the variables used in this study.

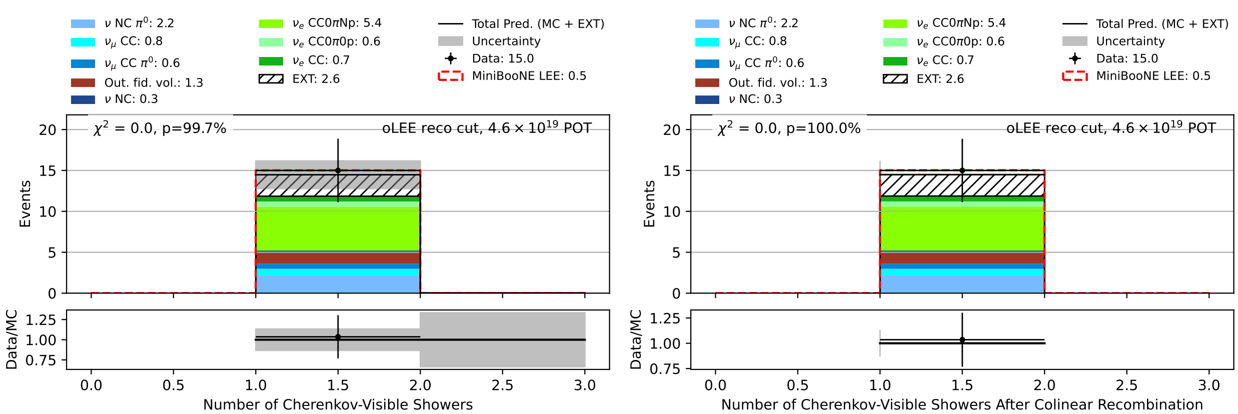

(a) nshr_visible (b) nshr_mB_vis

Figure C.1: The open data plots for nshr_visible (left) and nshr_mB_vis (right) with the NUE pre-selection and all 4 selections applied.

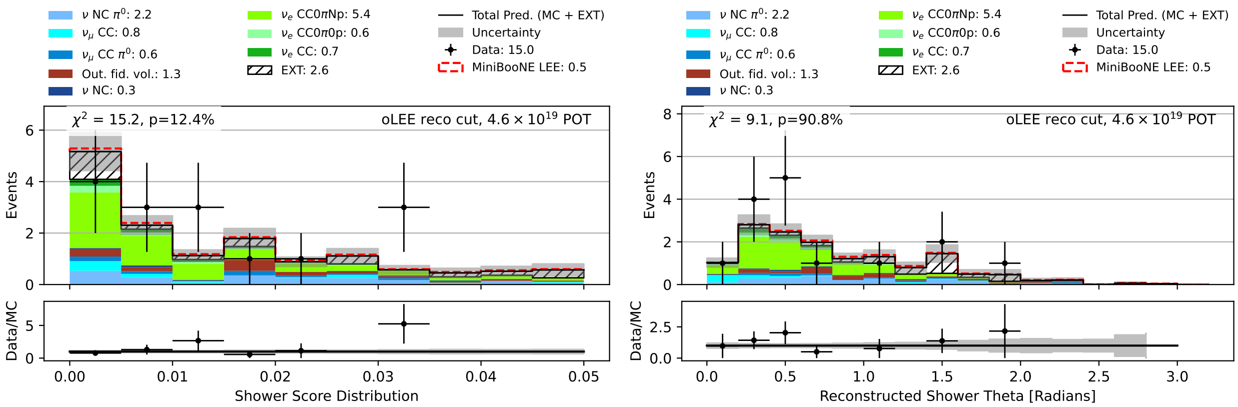

(a) shr_score (b) shr_theta

Figure C.2: The open data plots for shr_score (left) and shr_theta (right) with the NUE pre-selection and all 4 selections applied.

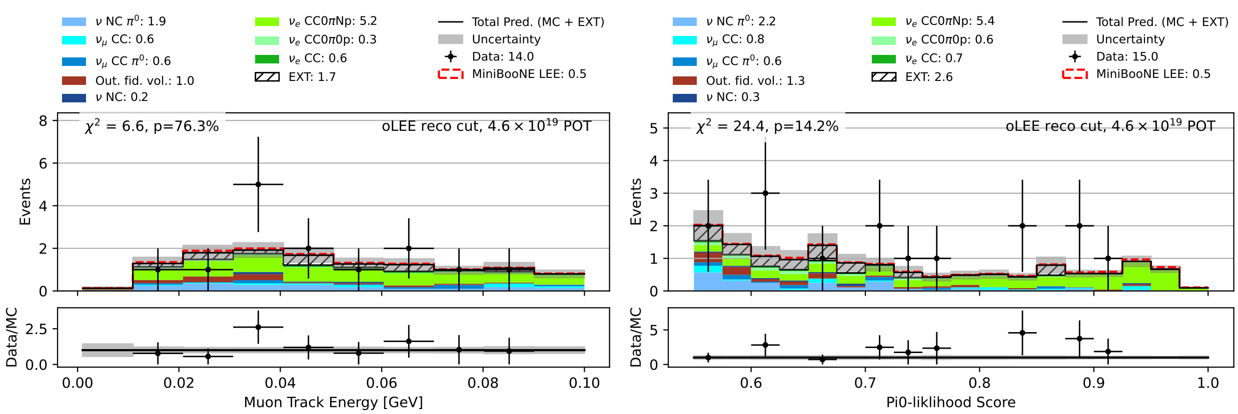

(a) trk_energy_muon (b) pi0_score

Figure C.3: The open data plots for trk_energy_muon (left) and pi0_score (right) with the NUE pre-selection and all 4 selections applied.

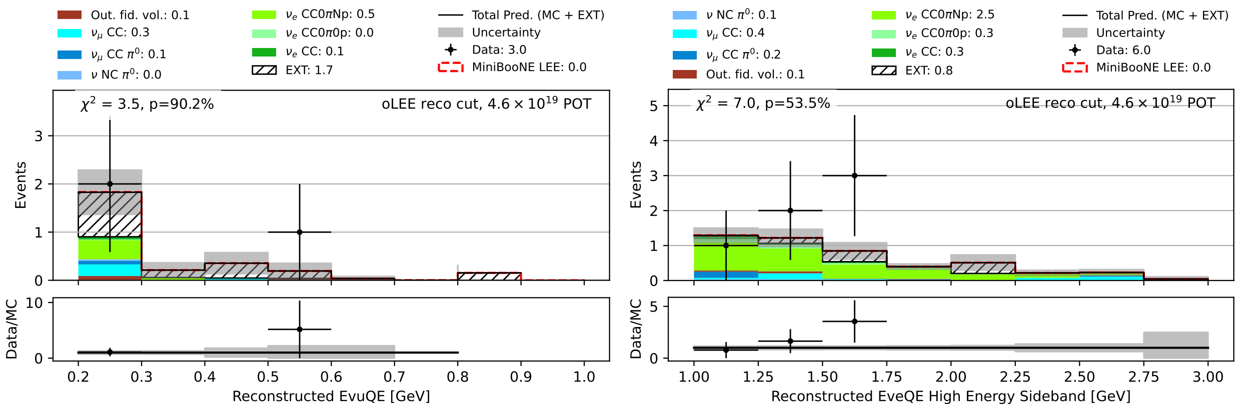

(a) reco_EvQElu (b) reco_EvQEle High Energy Sideband

Figure C.4: The open data plots for reco_EvQElu (left) and reco_EvQEle high energy side-band (right). THe reco_EvQEle variable has the NUE pre-selection and all 4 selections applied, but the reco_EvQElu variable only has the NUE pre-selection and selections 1 and 4 applied.

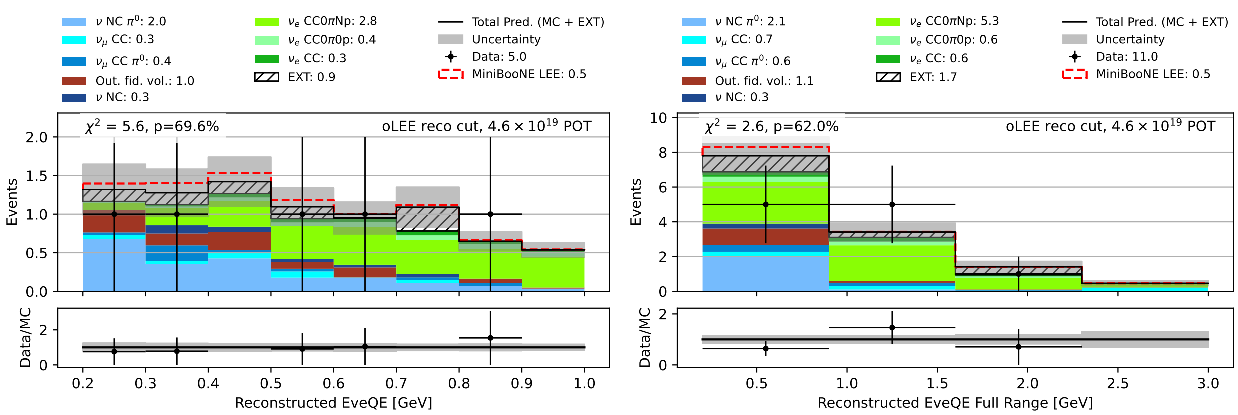

(a) reco_EvQEle Signal Region (b) reco_EvQEle Full Range Sensitivity Binned

Figure C.5: The open data plots for the reco_EvQEle signal region (left) and full range with sensitivty binning (right) with the NUE pre-selection and all 4 selections applied.

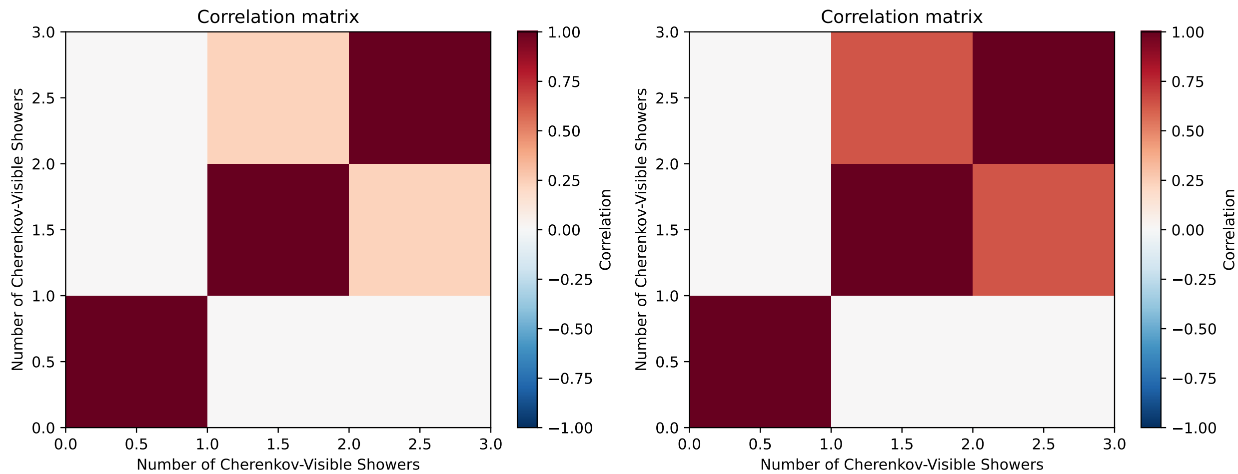

(a) Monte Carlo (b) Monte Carlo High Energy Sideband

Figure C.6: The correlation matrices for nshr_visible full Monte Carlo (left) and high energy sideband (right) with the NUE pre-selection and all 4 selections applied.

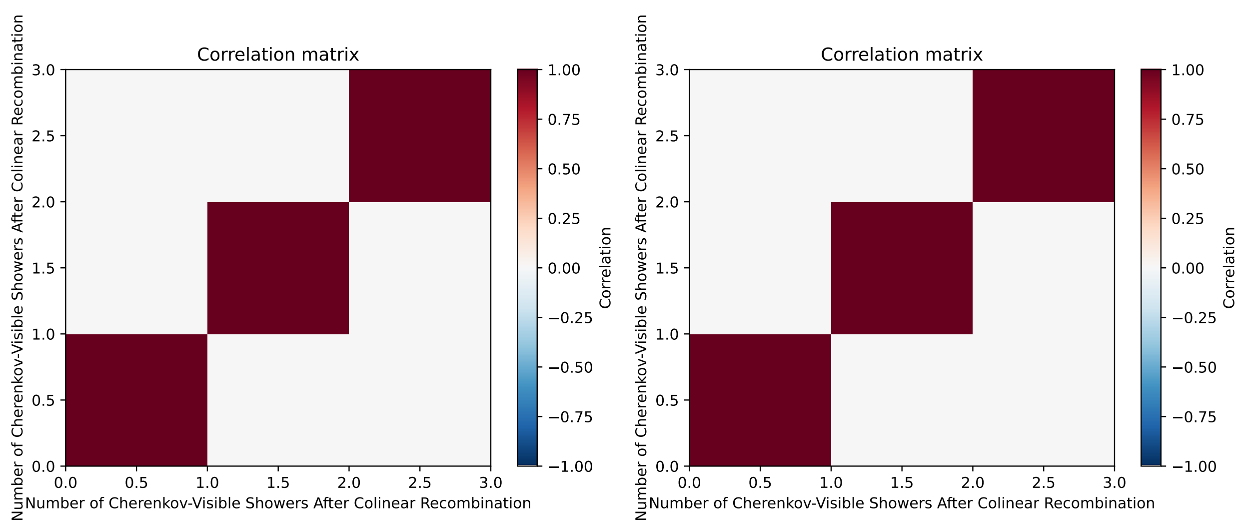

(a) Monte Carlo (b) Monte Carlo High Energy Sideband

Figure C.7: The correlation matrices for nshr_mB_vis full Monte Carlo (left) and high energy sideband (right) with the NUE pre-selection and all 4 selections applied.

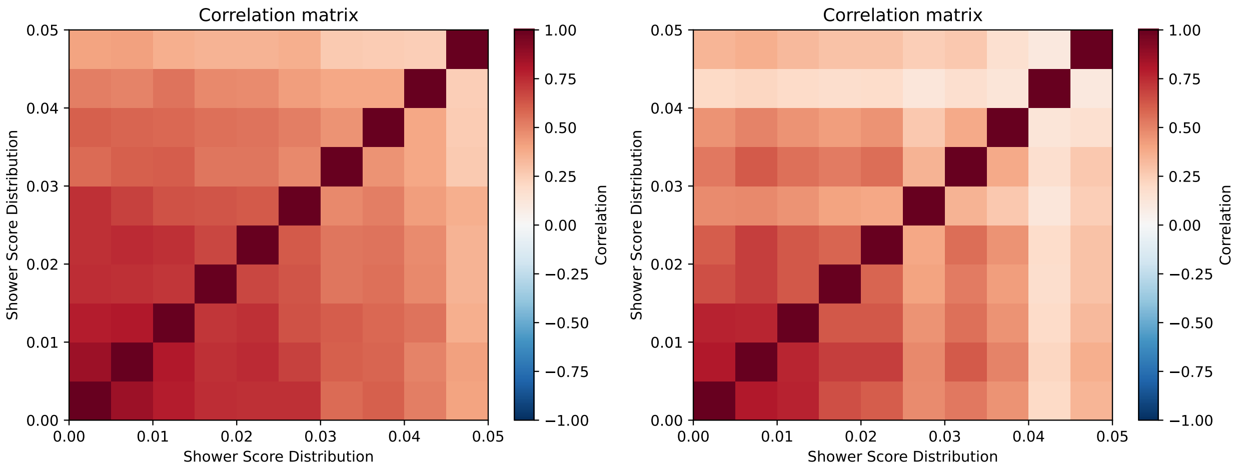

(a) Monte Carlo

(b) Monte Carlo High Energy Sideband

Figure C.8: The correlation matrices for shr_score full Monte Carlo (left) and high energy sideband (right) with the NUE pre-selection and all 4 selections applied.

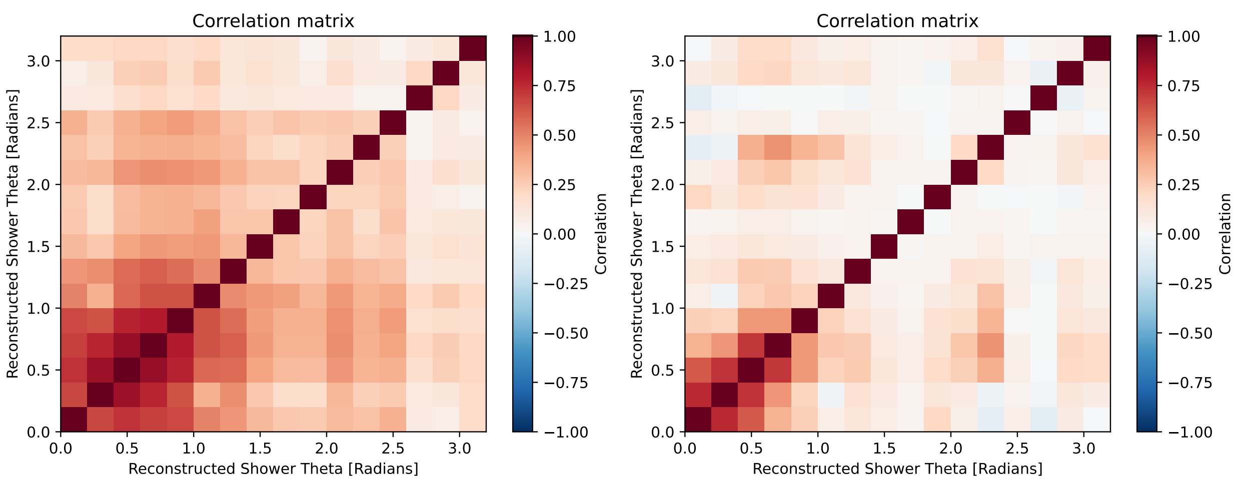

(a) Monte Carlo

(b) Monte Carlo High Energy Sideband

Figure C.9: The correlation matrices for shr_theta full Monte Carlo (left) and high energy sideband (right) with the NUE pre-selection and all 4 selections applied.

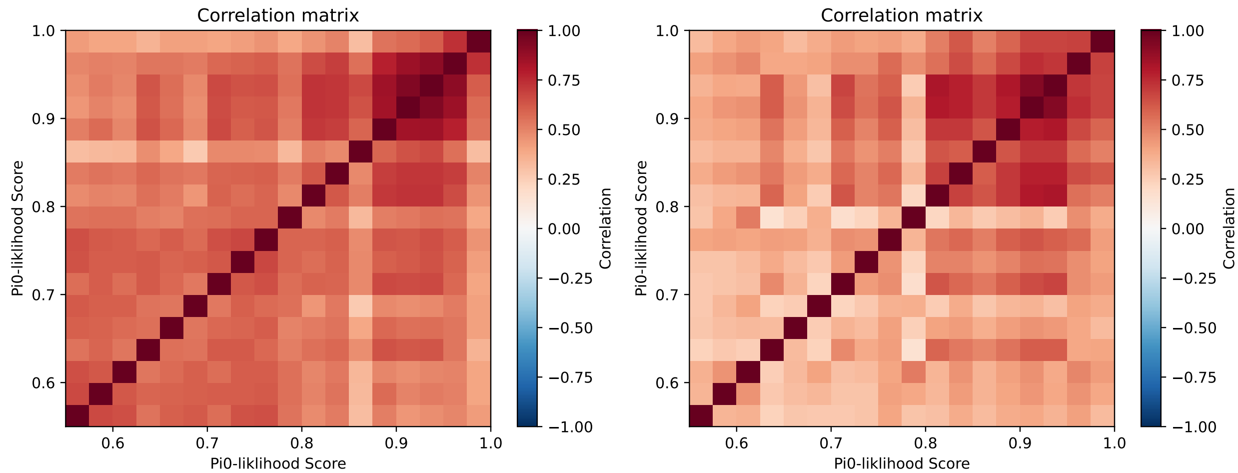

(a) Monte Carlo

(b) Monte Carlo High Energy Sideband

Figure C.10: The correlation matrices for pi0_score full Monte Carlo (left) and high energy sideband (right) with the NUE pre-selection and all 4 selections applied.

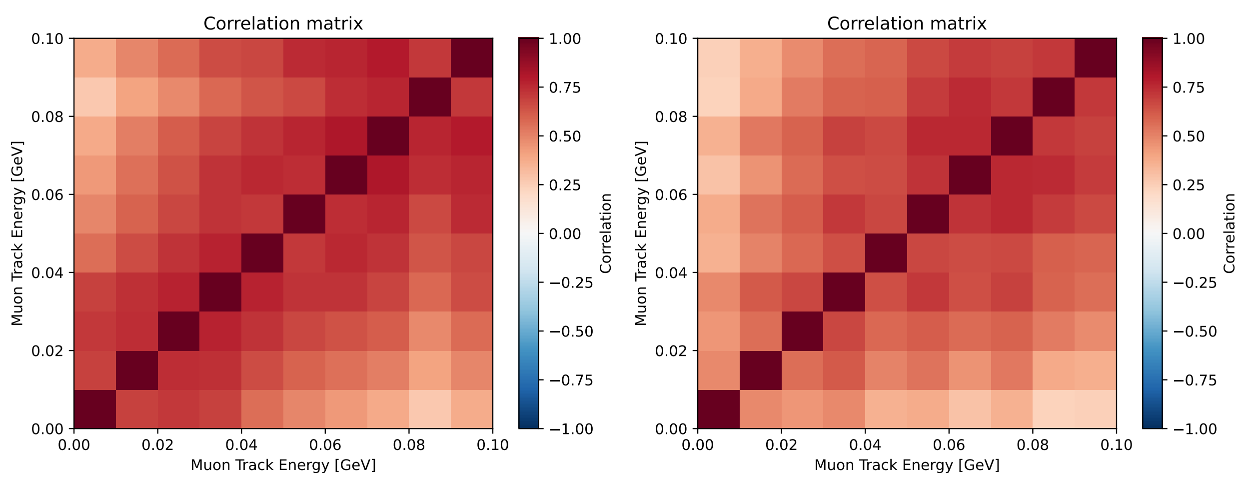

(a) Monte Carlo

(b) Monte Carlo High Energy Sideband

Figure C.11: The correlation matrices for trk_energy_muon full Monte Carlo (left) and high energy sideband (right) with the NUE pre-selection and all 4 selections applied.

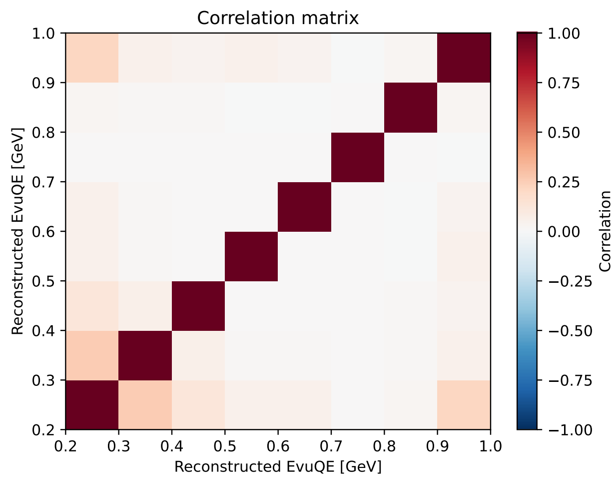

(a) Monte Carlo

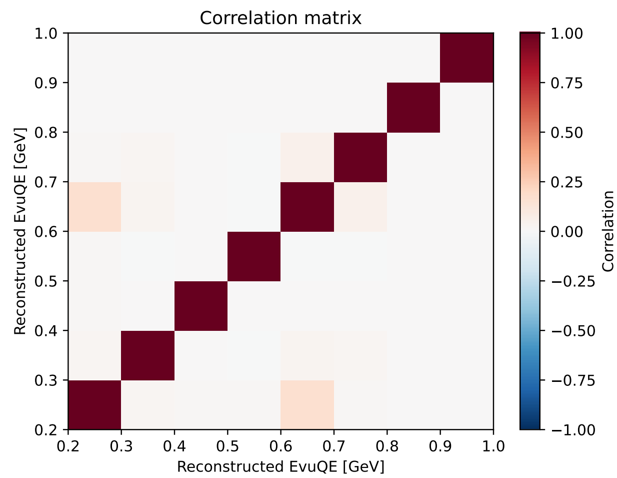

(b) Open Data

Figure C.12: The correlation matrices for reco_EvQElu full Monte Carlo (left) and open data (right) with the NUE pre-selection and selections 1 and 4 applied.

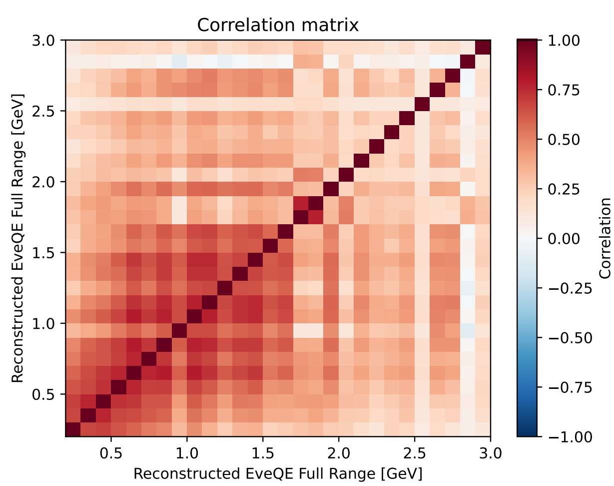

(a) Monte Carlo Full Range

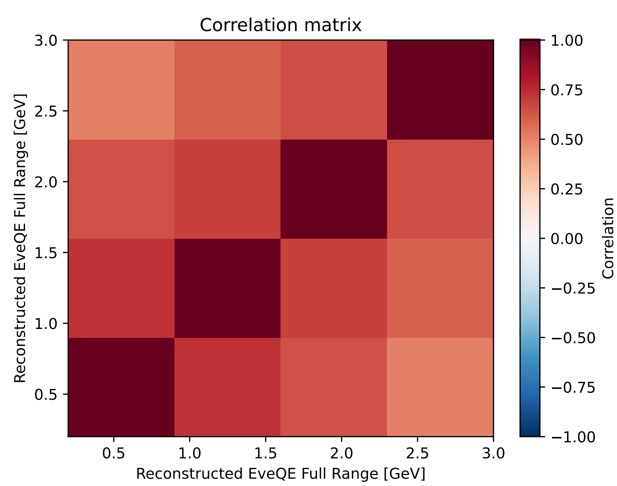

(b) Monte Carlo Sensitivity Binned

Figure C.13: The correlation matrices for reco_EvQEle full range Monte Carlo (left) and Monte Carlo sensitivity binned (right) with the NUE pre-selection and all 4 selections applied.

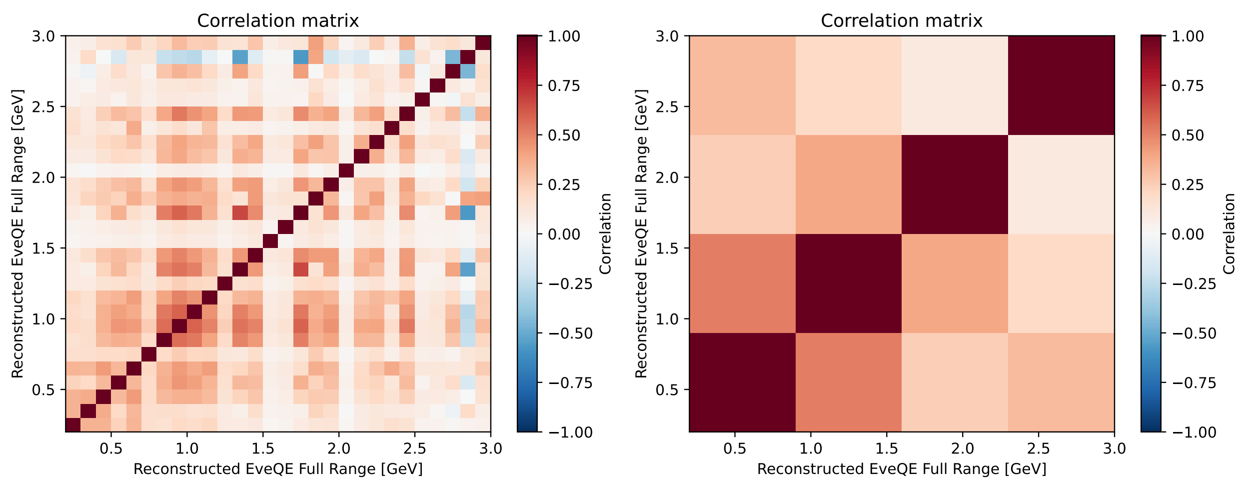

(a) Open Data Full Range

(b) Open Data Sensitivity Binned

Figure C.14: The correlation matrices for reco_EvQEle full range open data (left) and open data sensitivity binned (right) with the NUE pre-selection and all 4 selections applied.